

Synthesis, Biological, and Molecular Docking Studies on 4,5,6,7-Tetrahydrobenzo[*b*]thiophene Derivatives and Their Nanoparticles Targeting Colorectal Cancer

Shimaa Kamal, Hamed Ahmed Derbala, Seham Soliman Alterary, Abir Ben Bacha, Mona Alonazi, Mohamed Kandeel El-Ashrey, and Nahed Nasser Eid El-Sayed*



Cite This: *ACS Omega* 2021, 6, 28992–29008



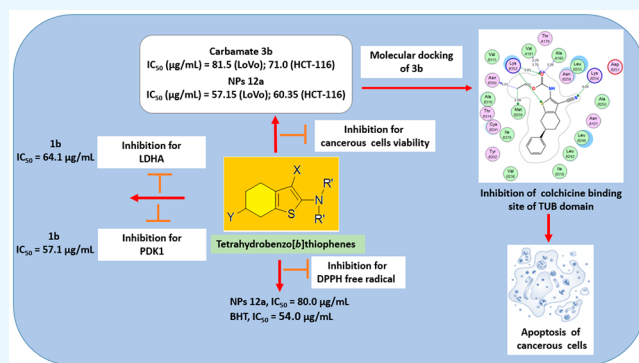
Read Online

ACCESS |

Metrics & More

Article Recommendations

ABSTRACT: Initiation of colorectal carcinogenesis may be induced by chromosomal instability caused by oxidative stress or indirectly by bacterial infections. Moreover, proliferating tumor cells are characterized by reprogrammed glucose metabolism, which is associated with upregulation of PDK1 and LDHA enzymes. In the present study, some 4,5,6,7-tetrahydrobenzo[*b*]thiophene derivatives in addition to Fe₃O₄ and Fe₃O₄/SiO₂ nanoparticles (NPs) supported with a new Schiff base were synthesized for biological evaluation as PDK1 and LDHA inhibitors as well as antibacterial, antioxidant, and cytotoxic agents on LoVo and HCT-116 cells of colorectal cancer (CRC). The results showed that compound **1b** is the most active as PDK1 and LDHA inhibitor with IC₅₀ values (μg/mL) of 57.10 and 64.10 compared to 25.75 and 15.60, which were produced by the standard inhibitors sodium dichloroacetate and sodium oxamate, respectively. NPs12a,b and compound **1b** exhibited the strongest antioxidant properties with IC₅₀ values (μg/mL) of 80.0, 95.0, and 110.0 μg/mL, respectively, compared to 54.0 μg/mL, which was produced by butylated hydroxy toluene. Moreover, NPs12a and carbamate derivative **3b** exhibited significant cytotoxic activities with IC₅₀ values (μg/mL) of 57.15 and 81.50 (LoVo cells) and 60.35 and 71.00 (HCT-116 cells). Thus, NPs12a and compound **3b** would be considered as promising candidates suitable for further optimization to develop new chemopreventive and chemotherapeutic agents against these types of CRC cell lines. Besides, molecular docking in the colchicine binding site of the tubulin (TUB) domain revealed a good binding affinity of **3b** to the protein; in addition, the absorption, distribution, metabolism, and excretion (ADME) analyses showed its desirable drug-likeness and oral bioavailability characteristics.



INTRODUCTION

Colorectal cancer (CRC) is the third most commonly diagnosed malignancy and the second leading cause of cancer death globally.¹ In Saudi Arabia, it is ranked as the first cancer type in males and the third in females.²

CRC is a complex disease that results from accumulated genetic and epigenetic changes, which inactivate tumor suppressor genes and activate oncogenes and eventually initiate tumorigenesis.³

Several studies have shown that microbial dysbiosis of certain bacterial species such as *Streptococcus bovis*, *Helicobacter pylori*, enterotoxigenic *Bacteroides fragilis* (ETBF), *Escherichia coli* (*E. coli*), and *Enterococcus faecalis* (*E. faecalis*) may indirectly promote colorectal carcinogenesis via epigenome dysregulation.^{4–7}

Further, throughout tumor progression, the neoplastic cells preferentially rely on glycolysis instead of oxidative phosphorylation (OXPHOS), which is known as the “Warburg effect”,

in order to fuel their increased bioenergetic demands for survival, infinite proliferation, invasion, and metastasis.⁸ This metabolic switch is associated with overexpression of pyruvate dehydrogenase kinase (PDK-1)⁹ and lactate dehydrogenase A (LDHA).¹⁰ PDK-1 inhibits the multi-enzyme pyruvate dehydrogenase complex (PDC) to decrease the level of pyruvate in mitochondria, which in turn limits the OXPHOS and blocks the production of mitochondrial reactive oxygen species (ROS), leading to survival of cancerous cells.¹¹ Similarly, LDHA restrains mitochondrial supply of pyruvate

Received: July 30, 2021

Accepted: September 29, 2021

Published: October 25, 2021



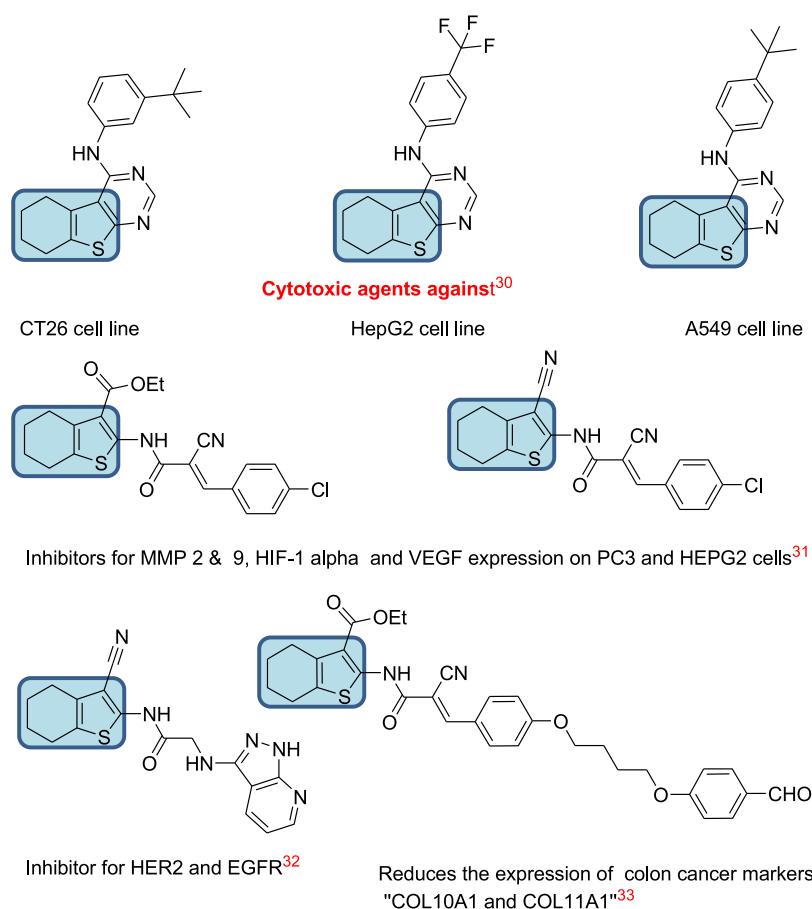


Figure 1. Examples of reported 4,5,6,7-tetrahydrobenzo[*b*]thiophene derivatives as anticancer agents against various therapeutic targets.

and catalyzes its conversion to lactate.¹² The produced lactate facilitates tumor survival, growth, and metastasis via suppression of host immune surveillance, tumor resistance, and upregulation of various angiogenesis-stimulating molecules.¹³ Accordingly, inhibitions of PDK-1¹⁴ and LDHA¹⁵ have been emerged as therapeutic strategies against cancer.^{16,17}

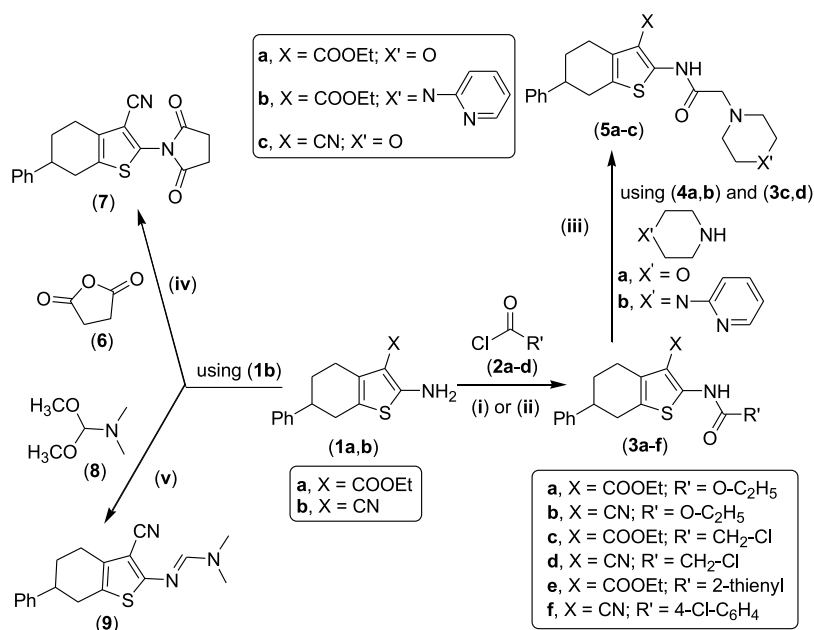
It is noteworthy to indicate that the enhancement of the Warburg effect is attributed to accumulated abnormalities resulting from mutations in genomic DNA¹⁸ and mitochondrial DNA.¹⁹ These mutations augment the generation of ROS, which interfere with inflammatory signaling leading to activation of inflammation,²⁰ inducing chromosomal instability (CIN), oxidative stress, and eventually the development of CRC and drug resistance.²¹

Taking together, the optimal reduction of CRC incidence, morbidity, and mortality will require concerted efforts to develop novel drug candidates that are capable of eliminating oxidative stress, eradicating bacteria, and/or inhibiting protumorigenic LDHA and PDK1 enzymes. In this regard, thiophene derivatives are extensively explored in the field of drug design and development as antioxidant,²² antibacterial,²³ and anticancer agents.^{24–29} In particular, 4,5,6,7-tetrahydrobenzo[*b*]thiophene derivatives have been recognized as promising anticancer agents.³⁰ Many of them (Figure 1) have produced their antiproliferative effects through targeting metalloproteinases 2 and 9 (MMP 2 and 9), HIF-1 α and the vascular endothelial growth factor receptor,³¹ the epidermal growth factor receptor (EGFR), human EGFR-related receptor 2 (HER2),³² and the colon cancer-related genes, namely,

collagen type X α 1 (COL10A1) and collagen type XI α 1 (COL11A1).³³

Moreover, nanotechnology has gained much interest in the field of medicinal chemistry because of advantages such as reduced doses of bioactive molecules, targeted delivery,³⁴ and enhanced bioavailability.³⁵ Indeed, thiophene derivatives loaded onto nanoparticles (NPs) displayed improved solubility and selectivity for cancerous cells compared to unmodified controls.^{34,36}

Based on the promising anticancer activities of various tetrahydrobenzo[*b*]thiophene derivatives and as a continuation to our recent investigations to develop new anti-CRC agents,^{37,38} herein, we aim to describe the synthesis and characterization of a new series of 4,5,6,7-tetrahydrobenzo[*b*]thiophene-based carbamates, amides, acetamides, a cyclic imide, a formamidine, and a Schiff base. The later product was used as a capping agent to prepare thiophene-Fe₃O₄ and thiophene-Fe₃O₄/SiO₂ NPs. All the synthesized compounds were evaluated as PDK-1 and LDHA inhibitors as well as antioxidant and antibacterial agents. The most bioactive candidates were screened as cytotoxic agents against LoVo and HCT-116 cells of CRC. Target identification and *in silico* molecular docking were carried out based on structural similarity between the previously reported antitumor compounds and the promising cytotoxic candidate to elucidate the mechanism underlying the observed antineoplastic effects.

Scheme 1^a

^aReagent and conditions: (i) ClCOOEt, reflux 10 h; (ii) dry CHCl₃, 0 °C, TEA, R'COCl, stirring 1 h, warm up to r.t., reflux 16 h; (iii) CH₃OH, reflux 10 h; (iv) NaOAc, oil bath at 200 °C 2 h; (v) dry xylene, reflux 10 h.

RESULTS AND DISCUSSION

Synthesis of 4,5,6,7-Tetrahydrobenzo[*b*]thiophene Derivatives. The synthetic routes toward the target compounds are outlined in Scheme 1. Initially, the starting materials 2-amino-6-phenyl-4,5,6,7-tetrahydrobenzo[*b*]thiophene-3-carboxylic acid ethyl ester **1a** and 2-amino-6-phenyl-4,5,6,7-tetrahydrobenzo[*b*]thiophene-3-carbonitrile **1b** were allowed to react with some active carbonyl compounds, namely, ethyl chloroformate **2a**, chloroacetyl chloride **2b**, thiophene-2-carbonyl chloride **2c**, and 4-chlorobenzoyl chloride **2d** under different reaction conditions. These reactions produced a series of 6-phenyl-4,5,6,7-tetrahydrobenzo[*b*]thiophene derivatives tethered with carbamate **3a,b**, chloroacetamide **3c,d**, and amide **3e–f** functionalities, respectively.

Subsequent condensation of chloroacetamides **3c,d** with morpholine **4a** and 1-(pyridin-2-yl)piperazine **4b** led to nucleophilic displacement of the chloride anion by these secondary amines with the formation of the corresponding new thiophene-based morphino and piperazino derivatives **5a–c**.

Moreover, compound **1b** was converted to the thienopyrroindione **7** and *N,N*-dimethylformamidinium derivative **9** via reaction with succinic anhydride **6** and DMF-DMA **8**, respectively.

Characterization of 4,5,6,7-Tetrahydrobenzo[*b*]thiophene Derivatives. The structures of all the newly synthesized products were deduced on the basis of their spectroscopic data as explained using representative examples.

For example, the infra-red (IR) spectrum of carbamate **3b** revealed the presence of the stretching absorption bands at $\nu_{\max}/\text{cm}^{-1} = 3221, 2219, \text{ and } 1725$ attributable to NH, CN, and CO groups, respectively. The ¹H NMR (300 MHz, DMSO-*d*₆) spectrum lacked the signal at $\delta_{\text{H}} = 7.01$ ppm due to the primary amino group of the starting material, and it exhibited three new characteristic signals at $\delta_{\text{H}} = 1.22, 4.21, \text{ and } 11.18$ ppm as follows: a three-proton triplet and a two-

proton quartet with coupling constants $J = 7.1$ Hz in addition to a one-proton singlet, which are attributed to the methyl, methylene, and amidic NH groups, respectively. Moreover, the ¹³C NMR (75 MHz, DMSO-*d*₆) spectrum displayed 13 signals as expected due to the 3-cyano-6-phenyl-4,5,6,7-tetrahydrobenzo[*b*]thiophene core in addition to 3 signals at $\delta_{\text{C}} = 14.31, 61.78, \text{ and } 153.57$ ppm due to the CH₃, CH₂, and CO groups, respectively. Last, the mass spectrum of this compound showed the molecular ion peak [$M^+ + 2$] at $m/z = 328.41$ (26%) for C₁₈H₁₈N₂O₂S in addition to the base peak at $m/z = 123.84$.

Furthermore, the IR spectrum of **5b** exhibited absorption bands at $\nu_{\max}/\text{cm}^{-1} = 3222, 1724, 1662, \text{ and } 1597$ attributable to NH, C=O-ester, C=O-amidic, and C=N groups, respectively. The ¹H NMR (300 MHz, DMSO-*d*₆) spectrum confirmed the insertion of the (pyridin-2-yl)piperazine moiety, which exhibited a characteristic apparent singlet signal integrating to four protons at $\delta_{\text{H}} = 3.60$ ppm due to two of the four CH₂-N groups of the piperazine ring. The four protons of the remaining CH₂-N groups are overlapped with the five protons of the cyclohexene ring at $\delta_{\text{H}} = 2.46\text{--}3.04$ ppm. In addition, the four protons of the pyridine ring exhibited four signals as follows: a one-proton multiplet, a one-proton doublet with coupling constant $J = 8.1$ Hz, an apparent one-proton triplet of doublet with coupling constant values $J = 8.1$ and 2.4 Hz, and a one-proton multiplet at $\delta_{\text{H}} = 6.60\text{--}6.70, 6.84, 7.56, \text{ and } 8.10\text{--}8.20$ ppm, respectively. Similarly, the ¹³C NMR (75 MHz, DMSO-*d*₆) spectrum indicated the piperazinopyridinyl moiety as two signals at $\delta_{\text{C}} = 45.00$ and 52.62 ppm attributable to the four methylene groups of the piperazine ring in addition to five signals belonging to the five sp²-carbons of the pyridine ring, which were detected among the fifteen signals in the aromatic region at $\delta_{\text{C}} = 107.16, 111.30, 113.11, 125.61, 126.24, 126.83, 128.37, 130.22, 137.56, 145.67, 146.06, 147.57, 158.92, 164.86 \text{ and } 167.95$ ppm. Moreover, its mass spectrum showed the molecular ion peak

$[M^+ + 2]$ at $m/z = 506.41$ (24%) for $C_{28}H_{32}N_4O_3S$ and the base peak at $m/z = 369.47$.

Analogously, the IR spectrum of the fromamidine derivative **9** missed the absorption band due to the primary amino group of its precursor **1b** and displayed a new stretching absorption band at $\nu_{\max}/\text{cm}^{-1} = 1628 \text{ cm}^{-1}$ corresponding to the $C=N$ group. The ^1H NMR (300 MHz, $\text{DMSO-}d_6$) spectrum confirmed the presence of the dimethyl formamidine moiety $[=CHN(\text{CH}_3)_2]$, which exhibited three singlet signals at $\delta_{\text{H}} = 2.98, 3.08, \text{ and } 7.96$ ppm attributable to the two methyl groups and the azomethine group, respectively. ^{13}C NMR (75 MHz, $\text{DMSO-}d_6$) disclosed the presence of the two methyl groups at $\delta_{\text{C}} = 34.62$ and 38.81 ppm and the azomethine carbon at $\delta_{\text{C}} = 155.28$ ppm. Additionally, the mass spectrum of this compound revealed the presence of the molecular ion peak $[M^+ + 2]$ at m/z (%) = 311.49 (57), corresponding to the molecular formula of $C_{18}H_{19}N_3S$, and the base peak at $m/z = 93.18$.

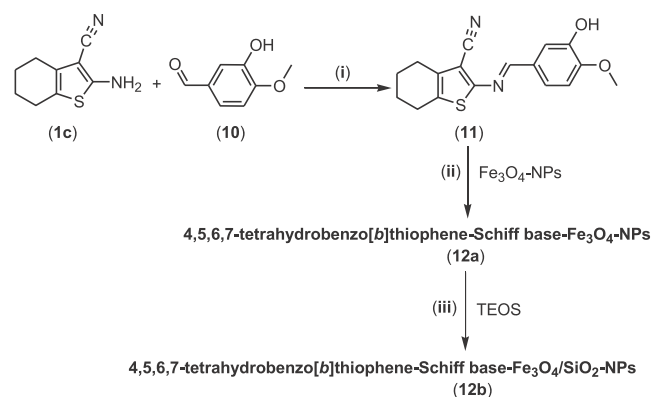
Synthesis and Characterization of Thiophene- Fe_3O_4 and Thiophene- $\text{Fe}_3\text{O}_4/\text{SiO}_2$ NPs. It is well established that iron NPs possess enhanced antibacterial, antioxidant, and anticancer properties.³⁹ However, it is known that the magnetic NPs are unstable, especially under physiological conditions and in the presence of air. Therefore, protection of these NPs with suitable species is a very important challenge between chemists. Moreover, their physical and chemical properties are determined by their size, shape, composition, crystallinity, and structure. Consequently, the design of magnetic nanocrystals for biomedical applications needs to be well controlled in order to get magnetic NPs bearing ligands capable of bonding to specific receptors and having a specific narrow range of sizes and a high degree of biocompatibility. Therefore, to investigate the process of the formation of the nanosystem to examine its effect on the various biological activities, we have designed one compound as a representative example for future work. In this regard, Schiff bases have been acknowledged as excellent capping agents capable of inhibiting the overgrowth of NPs and preventing their aggregation/coagulation in colloidal synthesis.⁴⁰ In addition, Schiff bases have gained importance in medicinal and pharmaceutical fields due to their broad spectrum of biological activities like antimicrobial, anticancer, and antioxidant.⁴¹

Thus, in this study, the Schiff base 2-((3-hydroxy-4-methoxybenzylidene)amino)-4,5,6,7-tetrahydrobenzo[*b*]thiophene-3-carbonitrile **11** was designed and prepared to be used as a coating shell for the new NPs, which will be evaluated for their efficacy as preventive or therapeutic agents against CRC. Initially, condensation of 2-amino-4,5,6,7-tetrahydrobenzo[*b*]thiophene-3-carbonitrile **1c** with isovanillin **10** yielded the new Schiff base derivative **11** whose structure was confirmed based on its spectroscopic data. Thus, the IR spectrum revealed the disappearance of the characteristic stretching absorption band due to the primary amino group of **1c** associated with the emergence of the characteristic stretching absorption bands at $\nu_{\max}/\text{cm}^{-1} = 3403$ (broad) and 1595 cm^{-1} , attributable to the phenolic OH and $C=N$ groups, respectively. Similarly, ^1H NMR (300 MHz, $\text{DMSO-}d_6$) analysis provided a rigid support for the assigned structure based on the disappearance of the signal at $\delta = 6.94$ ppm of the NH_2 group of the precursor **1c**. Moreover, this spectrum displayed three new singlet signals at $\delta_{\text{H}} = 9.52, 8.36, \text{ and } 3.83$ ppm due to the phenolic OH, azomethine (CH=N-), and methoxy (OCH_3) groups, respectively. Additionally, the ^{13}C

NMR (75 MHz, $\text{DMSO-}d_6$) spectrum indicated the presence of the methoxy group at $\delta_{\text{C}} = 55.65$ ppm. Also, the sp^2 -carbons due to the azomethine group and phenyl ring were displayed in the region of $160.43\text{--}104.87$ ppm. Last, the mass spectrum of compound **11** showed the molecular ion peak $[M^+ + 3]$ at $m/z = 315.74$ (4%), $[M^+ + 2]$ at $m/z = 314.82$ (10%), and the base peak was observed at $m/z = 77.13$.

Afterward, the magnetite was prepared by coprecipitation method, and it was allowed to react with 4,5,6,7-tetrahydrobenzo[*b*]thiophene-Schiff base **11** to give aldimine- Fe_3O_4 (NPs**12a**). The latter product was coated with silica to generate aldimine- $\text{Fe}_3\text{O}_4/\text{SiO}_2$ nanoparticles (NPs**12b**) through stirring with tetraethoxysilane (TEOS), as shown in Scheme 2.

Scheme 2^a



^aReagent and conditions: (i) ethanol, glacial acetic acid catalytic amount, reflux 16 h; (ii) EtOH/ H_2O (70:30) mixture, Fe_3O_4 NPs, compound **11**, reflux with stirring 4 h at 70°C ; (iii) EtOH/ $\text{H}_2\text{O}/\text{NH}_3$ (30:10:1) mixture, Schiff base- Fe_2O_3 NPs **12a**, US stirring 30 min, 2.5 mL of TEOS, stirring 22 h.

A series of characterizations were applied to investigate the structures of the aldimine-NPs **12a,b**. First, the morphologies of Fe_3O_4 and $\text{Fe}_3\text{O}_4/\text{SiO}_2$ capped with the organic compound were analyzed by transmission electron microscopy (TEM, JEOL JEM-2100 F). A drop of the colloidal solutions of the prepared NPs in the ethanol solvent was placed onto copper grids and was allowed to dry for TEM testing. The TEM micrograph of the Fe_3O_4 -NPs **12a** showed a cubic shape with good monodispersity and a mean diameter of 15 ± 2 nm (Figure 2a). Some slight aggregations were observed from the magnified image, which can be attributed to the aggregation of individual particles due to an incomplete coating with the organic molecules. An increase in the size of magnetite NPs **12b** was observed as shown in Figure 2b due to the formation of a thin layer of SiO_2 , which acted as a shell to the Fe_3O_4 core.

Second, a Malvern Instruments Zetasizer (model 2000) was used to determine the particle sizes of Fe_3O_4 and $\text{Fe}_3\text{O}_4/\text{SiO}_2$ colloids in ethanol by the dynamic light scattering technique. The measurements indicated the lowered particle size and polydispersity index for Fe_3O_4 -NPs than for $\text{Fe}_3\text{O}_4/\text{SiO}_2$. These results are in agreement with the data obtained from TEM micrographs. The increase in particle size diameter for both Fe_3O_4 and $\text{Fe}_3\text{O}_4/\text{SiO}_2$ NPs compared with that obtained from TEM micrographs is due to the interaction between NPs in the ethanol solvent, which lead to the formation of some agglomerations (Figure 3a,b).

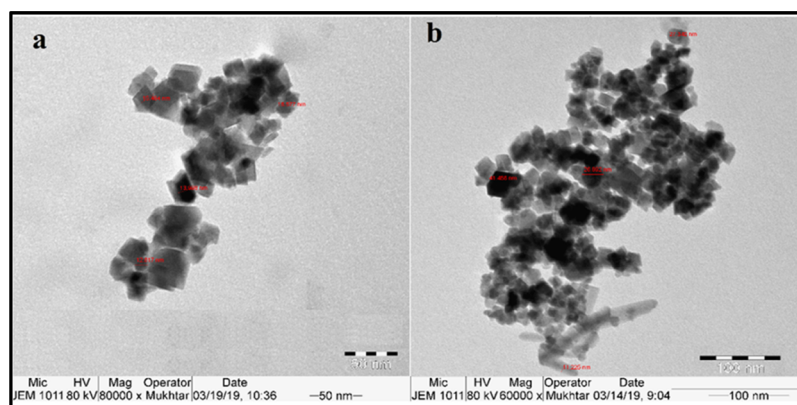


Figure 2. TEM images of aldimine NPs: (a) Fe_3O_4 and (b) $\text{Fe}_3\text{O}_4\text{-SiO}_2$.

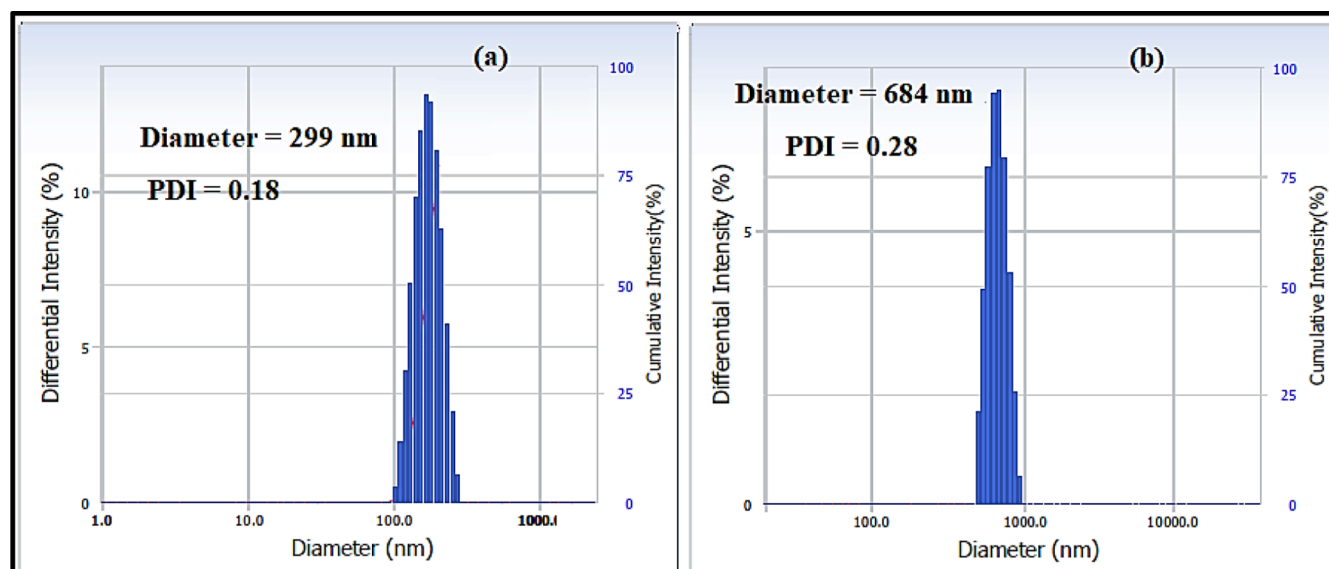


Figure 3. Particle size distribution of Fe-NPs capped with 2-((3-hydroxy-4-methoxybenzylidene)amino)-4,5,6,7-tetrahydrobenzo[*b*] thiophene-3-carbonitrile: (a) Fe_3O_4 -NPs and (b) $\text{Fe}_3\text{O}_4/\text{SiO}_2$ -NPs.

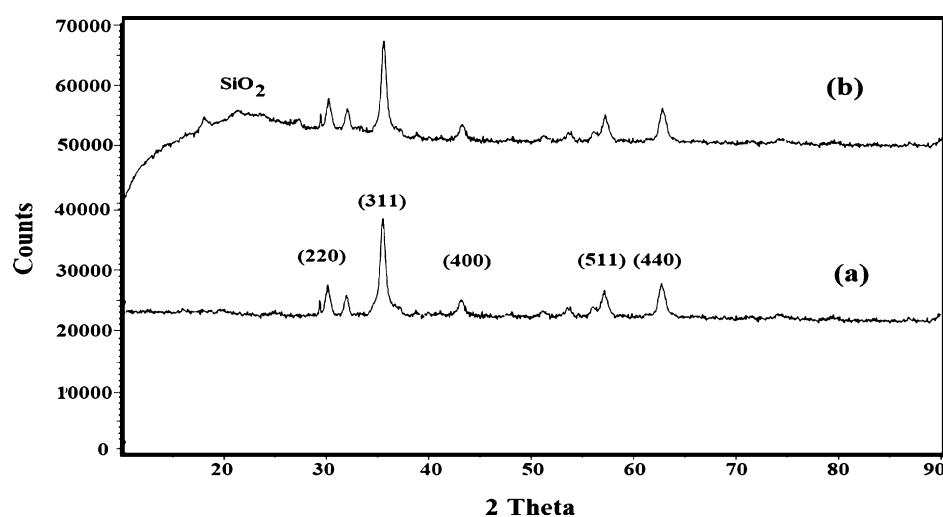


Figure 4. XRD patterns of 2-((3-hydroxy-4-methoxybenzylidene)amino)-4,5,6,7-tetrahydrobenzo[*b*] thiophene-3-carbonitrile loaded on (a) Fe_3O_4 and (b) $\text{Fe}_3\text{O}_4/\text{SiO}_2$.

Last, the crystal lattice structure and diffraction pattern of Fe_3O_4 -NPs capped with aldimine and with SiO_2 were analyzed by X-ray powder diffraction (XRD; BDX-3300 diffractometer

using $\text{Cu K}\alpha$ radiation of a wavelength of $\lambda = 1.5406 \text{ \AA}$). The XRD diffractograms of aldimine- Fe_3O_4 and aldimine- $\text{SiO}_2/\text{Fe}_3\text{O}_4$ (Figure 4a,b) confirmed the formation of magnetite

NPs without any other iron oxides. It was found that there are five characteristic peaks at 2-theta values of 30.5° (2 2 0), 35.9° (3 1 1), 43.5° (4 0 0), 57.3° (5 1 1), and 63.1° (4 4 0) to verify the crystalline structure of Fe₃O₄ particles, which is matched with the standard diffractions of Fe₃O₄ (JCPDS 89-4319). Also, the broad XRD peak at a low diffraction angle of 20–30° relates to the amorphous state of SiO₂ shells surrounding the Fe₃O₄-NPs.

Biological Investigation. The enzymatic inhibitory potencies of the synthesized derivatives were determined at a concentration of 100 µg/mL against both PDK1 and LDHA and compared to the inhibition efficiencies of the reference inhibitors sodium dichloroacetate and sodium oxamate at a concentration of 1 mM (1000 µM), respectively (Table 1 and Figure 5).

Table 1. Pyruvate Dehydrogenase Kinase-1 (PDK-1) and Lactate Dehydrogenase A (LDHA) Inhibitory Efficiencies of the Synthesized 4,5,6,7-Tetrahydrobenzo[*b*]thiophene Derivatives Determined at a Concentration of 100 µg/mL and Expressed in %^a

comp. #	mean inhibitory % at a concentration of 100 µg/mL ± SD	
	PDK-1	LDHA
1a	12.35 ± 1.91	19.25 ± 3.18
1b	87.00 ± 2.83	74.10 ± 2.97
1c	11.25 ± 3.18	23.15 ± 3.047
3a	21.50 ± 2.40	28.75 ± 2.057
3b	51.50 ± 3.54	19.30 ± 0.85
3c	37.95 ± 2.48	46.80 ± 2.55
3d	11.25 ± 1.77	24.85 ± 2.67
3e	18.40 ± 1.98	18.40 ± 1.98
3f	29.00 ± 2.83	27.50 ± 3.54
5a	41.00 ± 2.83	30.80 ± 1.70
5b	16.75 ± 1.63	34.70 ± 3.25
5c	21.40 ± 1.98	25.65 ± 2.33
7	35.90 ± 4.10	48.75 ± 5.30
9	36.50 ± 2.12	32.65 ± 2.33
11	23.70 ± 2.40	29.60 ± 1.98
12a	29.00 ± 2.83	40.15 ± 4.45
12b	23.75 ± 2.48	36.30 ± 3.25
sodium dichloroacetate	100.00 ± 0.00 at 150.92 µg/mL	
sodium oxamate		100.00 ± 0.00 at 111.03 µg/mL

^aSodium dichloroacetate (1 mM = 1000 µM = 150.92 µg/mL) and sodium oxamate (1 mM = 1000 µM = 111.03 µg/mL) were used as the standard inhibitors. Values of inhibitory percentage represent the mean ± SD of two different replicates.

The results of PDK1-assays revealed that compounds **1b** and **3b** were the most active with inhibition percentages of 87.0 and 51.50% relative to 100% produced by sodium dichloroacetate, respectively.

Similarly, compounds **1b**, and **7** demonstrated the highest inhibitory efficiencies of 74.10 and 48.75% against LDHA, respectively, compared with 100% by sodium oxamate.

The rest of the compounds exhibited poor inhibitory efficiencies ranging from 41.0 to 11.25% and from 46.80 to 18.40% against PDK1 and LDHA, respectively.

In the view of these results, the mean IC₅₀ values of compounds **1b**, **3b**, and **7** against both enzymes were determined in terms of µg/mL and µM and they were

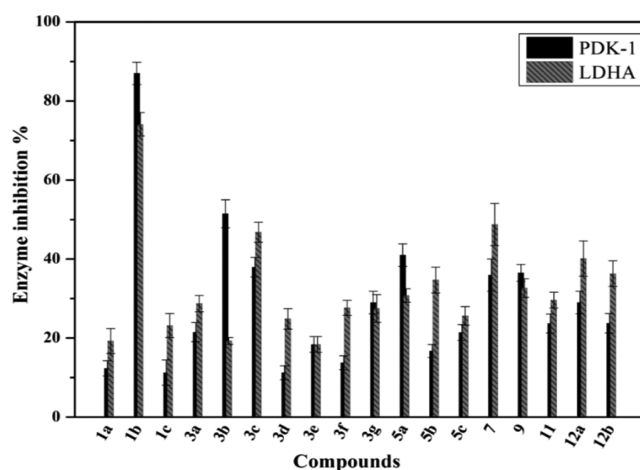


Figure 5. Enzymatic inhibitory assays of 4,5,6,7-tetrahydrobenzo[*b*]thiophene derivatives.

consistent with the observed percentages of inhibitory efficiencies as summarized in Table 2.

With regard to the antioxidant activities, they were assessed using DPPH radicals via determination of the percentages of scavenging activities of the studied compounds and butylated hydroxy toluene (BHT), which was used as the reference antioxidant drug at a 1000 µg/mL concentration. Additionally, the IC₅₀ values were deduced in µg/mL and µM as presented in Table 3 and Figures 6 and 7.

These experiments revealed that compounds **1b**, **12a**, **3d**, **12b**, and **3b** can be considered as promising antioxidant candidates as they exerted the strongest free-radical scavenging activities with efficiencies of 95.10 ± 1.27, 87.25 ± 1.77, 86.15 ± 1.63, 84.40 ± 2.40, and 79.95% ± 2.76 and the smallest IC₅₀ (µg/mL) values of 110.0 ± 14.14, 80.0 ± 14.14, 127.0 ± 9.90, 95.0 ± 7.07, and 130.0 ± 14.14, respectively, as compared with BHT, which displayed a radical scavenging potency of 95.30% ± 0.42 and an IC₅₀ value of 54.0 ± 5.66 µg/mL. The remaining compounds demonstrated good to moderate antioxidant properties with scavenging potencies (%) ranging from 73.95 ± 2.76 to 52.60 ± 2.26 and IC₅₀ (µg/mL) values ranging from 665.0 ± 21.21 to 210.0 ± 28.28.

The antibacterial evaluations were performed by determination of IC₅₀ (µg/mL and µM) against *E. faecalis* (ATCC 29122) and *E. coli* (ATCC 25922) using ampicillin as the reference antibiotic, as shown in Table 4 and Figure 8. The results indicated that the tested bacterial strains demonstrated varied sensitivities to the studied compounds, but none of them displayed stronger potency than ampicillin.

Considering the calculated IC₅₀ values (µg/mL) against *E. faecalis*, the compounds demonstrated higher values ranging from 44.10 ± 1.28 to 17.00 ± 0.28 with compounds **5c**, **12a**, and **12b** exhibiting the smallest values of 17.00 ± 0.28, 17.60 ± 0.57, and 18.60 ± 0.85, respectively, in comparison to 12.75 ± 1.06 by ampicillin.

Similarly, the tested compounds inhibited *E. coli* with IC₅₀ (µg/mL) values ranging from 22.25 ± 1.06 to 36.80 ± 1.70 with **12b** and **1a** being the most active candidates by exerting the lowest concentrations of 22.25 ± 1.06 and 24.90 ± 0.99, respectively, as compared with ampicillin, which exhibited 20.25 ± 1.77 µg/mL.

In the view of all performed biological experiments, the most active candidates **1b**, **3d**, **5c**, **12a**, and **12b** in addition to Schiff

Table 2. Summary of Inhibitory Efficiencies (%) and the Half-Maximal Inhibitory Concentration (IC₅₀) Expressed in μg/mL and μM of Compounds 1b, 3b, and 7 against PDK1 and LDHA^a

comp. # (MWt)	PDK1			LDHA		
	IC ₅₀ (μg/mL) ± SD	IC ₅₀ (μM)	mean % inhibition ± SD at 100 μg/mL	IC ₅₀ (μg/mL) ± SD	IC ₅₀ (μM)	mean % inhibition ± SD at 100 μg/mL
1b (254.35)	57.10 ± 2.97	224.49	87.00 ± 2.83	64.1 ± 4.10	252.01	74.10 ± 2.97
3b (326.41)	98.50 ± 4.95	301.76	51.50 ± 3.54	291.0 ± 5.66	891.52	19.30 ± 0.85
7 (336.41)	144.00 ± 5.66	428.05	35.90 ± 4.10	93.0 ± 2.83	276.45	48.75 ± 5.30
sodium dichloro-acetate (150.92)	25.75 ± 1.06	170.62	100.00% at 150.92 μg/mL = 1 mM = 1000 μM			
sodium oxamate (111.03)				15.6 ± 0.85	140.50	100.00% at 111.03 μg/mL = 1 mM = 1000 μM

^aResults are the mean values of two separate determinations ± SD.

Table 3. Evaluation of the Antioxidant Activities of the Synthesized 4,5,6,7-Tetrahydrobenzo[b]thiophene Derivatives by Determination of DPPH Free-Radical Scavenging Activity (%) at a Concentration of 1000 μg/mL and IC₅₀ Values Expressed as μg/mL and μM^a

comp. # (MWt)	mean scavenging activity (%) at 1000 μg/mL ± SD		mean IC ₅₀ (μg/mL) ± SD	mean IC ₅₀ (μM)
	1000 μg/mL ± SD	IC ₅₀ (μg/mL) ± SD		
1a (301.40)	63.35 ± 1.90	390.5 ± 13.44	1295.62	
1b (254.35)	95.10 ± 1.27	110.0 ± 14.14	432.47	
1c (178.25)	72.25 ± 1.77	332.5 ± 17.68	1865.35	
3a (373.47)	57.35 ± 1.91	665.0 ± 21.21	1780.60	
3b (326.41)	79.95 ± 2.76	130.0 ± 14.14	398.27	
3c (377.88)	63.15 ± 1.63	365.0 ± 21.21	965.92	
3d (330.83)	86.15 ± 1.63	127.0 ± 9.90	383.88	
3e (411.53)	52.60 ± 2.26	595.0 ± 21.21	1445.82	
3f (392.90)	58.25 ± 3.18	400.0 ± 14.14	1018.07	
5a (428.55)	61.05 ± 2.90	440.0 ± 28.28	1026.72	
5b (504.65)	73.95 ± 2.76	285.0 ± 21.21	564.74	
5c (381.49)	59.50 ± 2.12	525.0 ± 35.36	1376.18	
7 (336.41)	73.20 ± 2.55	222.5 ± 17.68	661.40	
9 (309.43)	69.20 ± 1.13	210.0 ± 28.28	678.67	
11 (312.39)	58.20 ± 1.13	332.5 ± 17.68	1064.37	
12a	87.25 ± 1.77	80.0 ± 14.14		
12b	84.40 ± 2.40	95.0 ± 7.07		
BHT (220.35)	95.30 ± 0.42	54.0 ± 5.66	245.06	

^aResults are the mean values of two separate determinations ± SD.

base **11** along with compounds **3b**, **7**, and **9** as representative examples for the newly introduced chemical functionalities on the starting amino thiophenes were further evaluated for their *in vitro* cytotoxic activities against HCT-116 and LoVo cell lines of CRC by determination of the percentages of residual viable cells after being exposed to each compound at a concentration of 100 μg/mL associated with utilization of 0.1% Triton X-100 in the assay medium and the assay medium as the positive and negative controls, respectively. The obtained results (Table 5 and Figure 9) indicated that the NPs **12a,b** and carbamate derivative **3b** were the most active by demonstrating the lowest cell viability percentages of 11.75 ± 1.06, 33.25 ± 1.77, and 35.50 ± 2.12 against LoVo cells, respectively.

Furthermore, the viability of HCT-116 cells was reduced to 15.75 ± 1.06, 28.00 ± 1.41, and 30.50 ± 2.12 by compounds **12a**, **3b**, and **12b**, respectively.

Although compound **1b** was recognized as the most active candidate against the PDK1 and LDHA enzymes (Table 2), it

did not demonstrate significant cytotoxicity against the examined cell lines (% cell viabilities of 56.50 ± 0.71 and 53.50 ± 2.12); thus, it is worthwhile to investigate its antitumor potential on different cancer types and cell lines in the future.

Contrarily, NPs **12a,b** and carbamate **3b**, which showed moderate to poor PDK1 and LDHA inhibitory efficiencies were found to be the most active cytotoxic candidates, implying that the observed antitumor properties would be resulted from the interaction of these compounds with other molecular targets.

Next, the IC₅₀ values expressed in μg/mL and μM of compounds **3b**, **7**, **9**, **11**, and **12a** against the tested HCT-116 and LoVo cell lines were calculated (Table 6). The NPs **12a** and carbamate **3b**, respectively, exerted the smallest values of 60.35 ± 2.76 and 71.00 ± 2.83 μg/mL (against HCT-116 cells) and 57.15 ± 2.48 and 81.5 ± 3.54 μg/mL (against LoVo cells).

Structure–Activity Relationship Studies. The structure–activity relationships of the newly synthesized 4,5,6,7-tetrahydrobenzo[b]thiophene derivatives can be derived on the basis of the results obtained from enzyme inhibition, antioxidant, antibacterial, and anticancer experiments as follows:

1. The enzymatic inhibitory activities against PDK-1 and LDHA were enhanced because of the presence of the primary amino group coupled with the nitrile group on the thiophene ring (compound **1b**). The transformation of the amino group to other functionalities reduced the efficiency by at least 1.5-fold as indicated by comparing the IC₅₀ values of compound **1b** with carbamate derivative **3** and cyclic imide analogue **7**.
2. The presence of the electron-donating amino group capable of H-bond formation (compound **1b**)⁴² and the formation of Fe₃O₄-NPs (compound **12a**)⁴³ and the Fe₃O₄-NPs coated by SiO₂ (compound **12b**) in addition to the insertion of chloroacetamide (in compound **3d**) and the carbamate (in compound **3b**)⁴⁴ moieties along with the presence of the nitrile group in the 4,5,6,7-tetrahydrobenzo[b]thiophene core is crucial for the potent free-radical scavenging capacities.
3. The antibacterial activity of the synthesized compounds was improved as a result of the formation of Fe₃O₄-NPs⁴⁵ (compound **12a**) and the transformation of the amino group to the morphino-acetamide moiety (in compound **5c**) against *E. faecalis* and the formation of Fe₃O₄-NPs coated by SiO₂⁴⁶ (compound **12b**) against *E. faecalis* and *E. coli*.

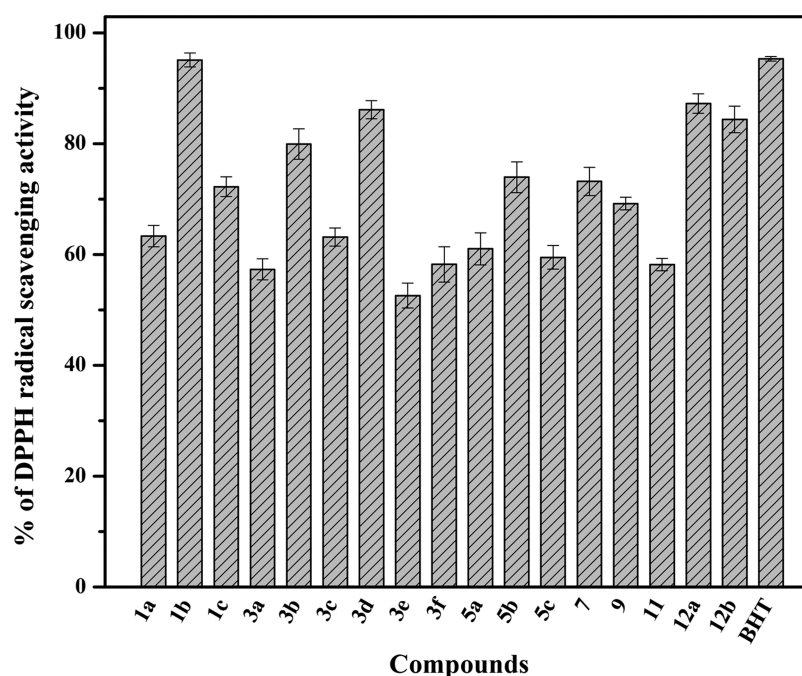


Figure 6. DPPH radical scavenging activity expressed as % for the synthesized 4,5,6,7-tetrahydrobenzo[*b*]thiophene derivatives and the reference antioxidant BHT at a concentration of 1000 $\mu\text{g/mL}$.

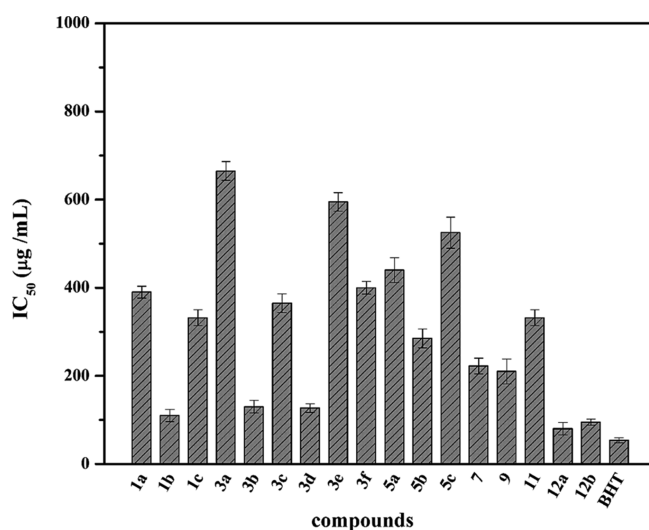


Figure 7. Antioxidant activities of the synthesized 4,5,6,7-tetrahydrobenzo[*b*]thiophene derivatives and the reference antioxidant BHT determined through calculations of the half-maximal inhibitory concentrations (IC_{50} values) expressed as $\mu\text{g/mL}$.

- The anticancer potency of the synthesized compounds was improved against LoVo and HCT-116 cells of CRC as a result of the formation of Fe_3O_4 -NPs (compound 12a) and Fe_3O_4 -NPs coated by SiO_2 ⁴⁷ (compound 12b) and by the insertion of the carbamate moiety⁴⁸ (in compound 3b).

Thus, our results are in accordance with the previously published data, which showed that the carbamate group is a structural motif in several anticancer drugs and prodrugs that are approved by the Food and Drug Administration (FDA) in USA and the European Medicines Agency (EMA), as shown in Figure 10.⁴⁸

For example, docetaxel is a carbamate containing an antineoplastic drug against breast, ovarian, and non-small cell lung cancers. It produces its chemotherapeutic action through interfering with several tumorigenic pathways. Thus, it induces programmed cell death (apoptosis) in cancer cells by binding to the antiapoptotic Bcl-2 (B-cell leukemia 2) protein and thus arresting its function. Also, it is considered as an antimicrotubule agent capable of destroying the cell's ability to use its cytoskeleton in a flexible manner through promoting microtubulin assembly and stabilizing the polymers against depolymerization. Further research indicated that docetaxel has been shown to inhibit angiogenesis.⁴⁹

Irinotecan is another key antineoplastic drug for metastatic CRC, which contains a carbamate moiety. The mechanism underlying its antitumor effect primarily depends on binding to topoisomerase I and inhibiting its action in addition to causing double-strand DNA breakage, which leads to irreversible inhibition of DNA synthesis, thus inducing arrest of the cell cycle in S-G2 leading to cell death.⁵⁰

Moreover, capecitabine (Xeloda) is an oral fluoropyrimidine carbamate prodrug against metastatic breast and colon cancers. It is selectively activated at the tumor site under the action of thymidine phosphorylase, which converts it to 5-fluorouracil (5-FU), which is further metabolized to the active metabolites to cause cell injury. This prodrug is absorbed intact through the gastrointestinal tract; thus, it provides protection against gut toxicity induced by 5-FU itself.⁵¹

Collectively, the carbamate group is considered as an important motif that increases the biological activity of different pharmacophoric scaffolds when it is introduced on them. This functional group allows modification of the pharmacokinetic properties of the compounds containing them through varying the substituents on its amino and carboxylate termini. Additionally, it improves their stability, potency, duration of action, and target specificity.⁴⁸

Table 4. Evaluation of the Antibacterial Activity of the Synthesized 4,5,6,7-Tetrahydro-benzo[*b*]thiophene Derivatives by Determination of IC₅₀ Values Expressed as μg/mL and μM^a

comp. # (Mwt)	<i>Enterococcus faecalis</i> (ATCC 29122)		<i>E. coli</i> (ATCC 25922)	
	mean IC ₅₀ (μg/mL) ± SD	mean IC ₅₀ (μM)	mean IC ₅₀ (μg/mL) ± SD	mean IC ₅₀ (μM)
1a (301.40)	44.10 ± 1.28	146.32	24.90 ± 0.99	82.61
1b (254.35)	21.20 ± 1.13	83.35	NS	NS
1c (178.25)	21.25 ± 1.06	119.21	26.25 ± 1.06	147.27
3a (373.47)	38.10 ± 1.27	102.01	27.05 ± 0.35	72.43
3b (326.41)	27.25 ± 1.06	83.48	NS	NS
3c (377.88)	26.15 ± 1.20	69.20	33.25 ± 1.06	87.99
3d (330.83)	40.60 ± 1.98	122.72	30.90 ± 1.56	93.40
3e (411.53)	37.30 ± 0.99	90.64	36.80 ± 1.70	89.42
3f (392.90)	42.00 ± 0.71	106.90	28.30 ± 1.70	72.03
5a (428.55)	26.65 ± 0.50	62.19	26.90 ± 0.57	62.77
5b (504.65)	24.75 ± 1.77	49.04	NS	NS
5c (381.49)	17.00 ± 0.28	44.56	NS	NS
7 (336.41)	28.10 ± 1.56	83.53	27.90 ± 2.26	82.93
9 (309.43)	34.20 ± 0.99	110.53	29.35 ± 1.20	94.85
11 (312.39)	39.35 ± 0.92	125.96	56.60 ± 1.98	181.18
12a	17.60 ± 0.57		26.20 ± 0.85	
12b	18.60 ± 0.85		22.25 ± 1.06	
Amp. (349.406)	12.75 ± 1.06	36.49	20.25 ± 1.77	57.96

^aResults are the mean values of two separate determinations ± SD. NS: not specified.

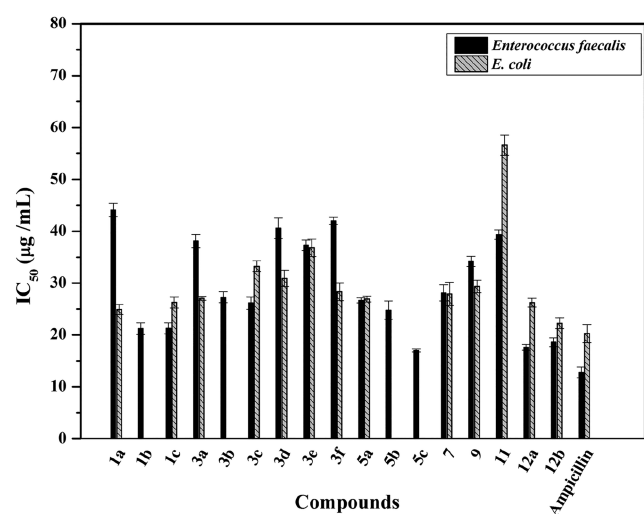


Figure 8. Antibacterial activities of the synthesized 4,5,6,7-tetrahydrobenzo[*b*]thiophene derivatives determined through the calculation of the half-maximal inhibitory concentrations, IC₅₀ values, expressed as μg/mL.

In Silico Molecular Docking Studies to Unveil the Underlying Molecular Mechanism of Cytotoxic Effects. Molecular docking of a chemical inhibitor in the active pocket of the proper molecular target is widely used as an approach to investigate the possible underlying antitumor mechanism of action. Microtubules are cellular polymers, which play diverse roles within the cell, including chromosomal segregation, cytokine and chemokine secretion, maintenance of the cell structure, protein trafficking, cell migration, and cell division. Thus, targeting tubulin dynamics is a promising approach for new chemotherapeutic agents. Compounds capable of disturbing microtubules by either stabilizing or destabilizing them would produce antiproliferative activity via enhancing mitotic arrest and cell apoptosis. At least three main binding sites in the tubulin protein, including colchicine, taxane, and

Table 5. Mean % of Viable LoVo and HCT-116 Cancerous Cells after Being Treated with Selected 4,5,6,7-Tetrahydrobenzo[*b*]thiophene Derivatives^a

comp. #	mean % of viable LoVo cells ± SD	mean % of viable HCT-116 cell ± SD
positive control Triton X-100 (0.1%)	0.00	0.00
negative control	99.50 ± 0.71	100.00 ± 0.00
1b	56.50 ± 0.71	53.50 ± 2.12
3b	35.50 ± 2.12	28.00 ± 1.41
3d	77.00 ± 2.83	65.50 ± 0.717
5c	79.50 ± 2.12	90.50 ± 2.12
7	51.50 ± 2.12	47.25 ± 1.06
9	71.80 ± 2.55	69.00 ± 1.41
11	63.75 ± 1.77	60.50 ± 2.12
12a	11.75 ± 1.06	15.75 ± 1.06
12b	33.25 ± 1.77	30.50 ± 2.12

^aResults are the mean values of two separate determinations ± SD.

vinca alkaloid, have been identified as targets for the anticancer drugs.⁵²

Due to the fact that the promising cytotoxic candidate 3b is a benzo[*b*]thiophene derivative with carbamate functionality, where both these structural units were found to inhibit tubulin polymerization, which in turn leads to irreversible damage to the tumor vasculature and eventually causes mitotic arrest and tumor necrosis,^{49,53} in the current study, the inhibitory potential of this compound against the tubulin (TUB) domain was studied using *in silico* molecular docking analyses to explore its underlying antitumor mechanism of action.

Initially, the docking setup was first validated by self-docking of the co-crystallized ligand (COL) in the vicinity of the binding site of the protein (Figure 11), the docking score (*S*) was −13.0770 kcal/mol, and the root-mean-square deviation (RMSD) value was 0.8996 Å, which is less than the cutoff value (2 Å) for the correct docking procedure.⁵⁴

Table 6. Half-Maximal Inhibitory Concentrations (IC_{50}) Expressed as $\mu\text{g/mL}$ and μM of the Active Cytotoxic Compounds against HCT-116 and LoVo Cells of CRC^a

comp. # (MWt)	LoVo cells		HCT-116	
	mean IC_{50} ($\mu\text{g/mL}$) \pm SD	mean IC_{50} (μM)	mean IC_{50} ($\mu\text{g/mL}$) \pm SD	mean IC_{50} (μM)
3b (326.41)	81.50 \pm 3.54	249.68	71.00 \pm 2.83	217.52
7 (336.41)	108.50 \pm 3.54	322.52	97.00 \pm 2.83	288.34
9 (309.43)	198.50 \pm 4.95	641.50	162.00 \pm 4.24	523.54
11 (312.39)	148.00 \pm 4.24	473.77	126.00 \pm 4.25	403.34
12a	57.15 \pm 2.48		60.35 \pm 2.76	

^aResults are the mean values of two separate determinations \pm SD.

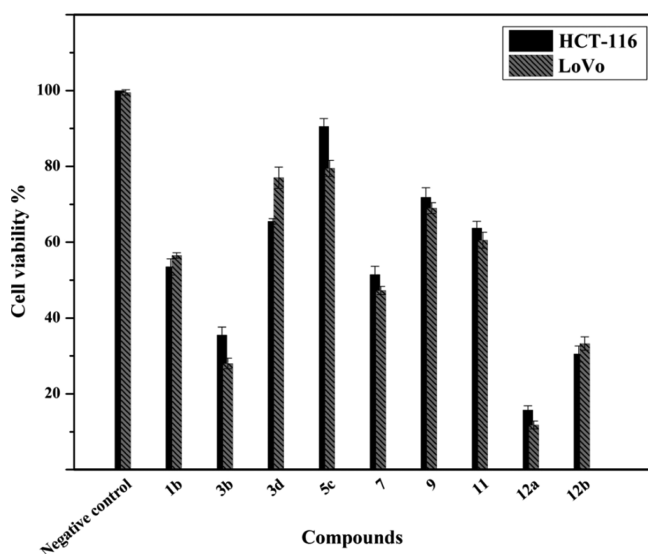


Figure 9. *In vitro* viability % of the LoVo and HCT-116 cancerous cells after being treated with selected 4,5,6,7-tetrahydrobenzo[*b*]-thiophene derivatives. The results are the mean values of two separate determinations \pm SD.

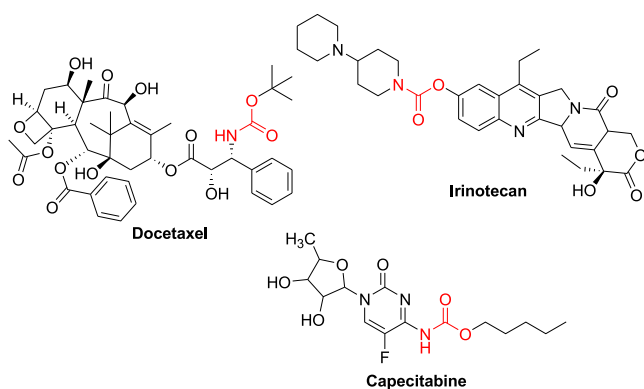


Figure 10. Examples of carbamate containing antineoplastic drugs.

Through examination of the binding interactions of colchicine (COL) to the active site of the protein, it showed strong hydrogen bond interactions with Ala-A180, Val-A181, Leu-B248, and Lys-B352 (Figure 12).

With regard to compound 3b, the docking results, which are summarized in Table 7 and Figure 13, showed that it exhibited a good binding score (-11.3097 kcal/mol), and it was capable of fitting inside the pocket of the target tubulin active site. The compound exhibited good binding interactions using the carbonyl group as a hydrogen bond acceptor with Ala-A180, Val-A181, and Lys-B352 residues. Moreover, the sulfur atom

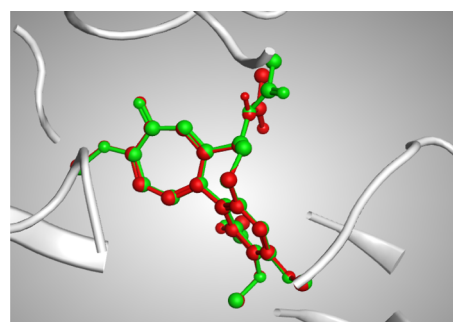


Figure 11. 3D representation of the superimposition of the co-crystallized ligand (red) and the docking pose (green) of COL in the active site of TUB.

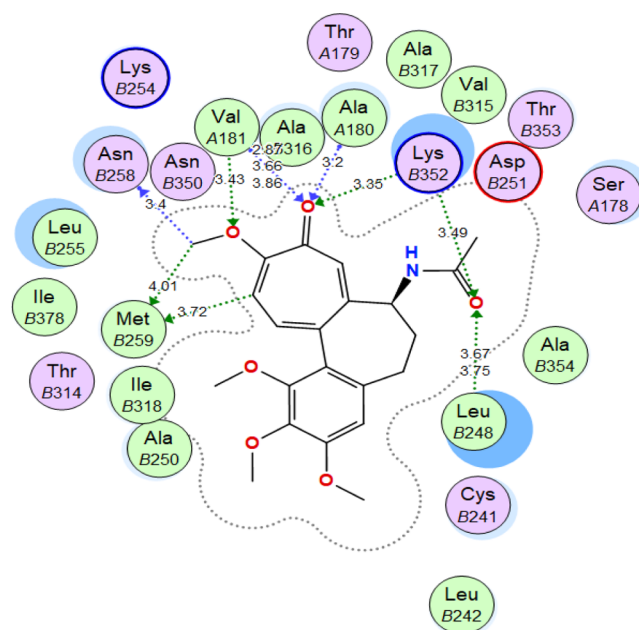


Figure 12. 2D interactions of COL within the TUB active site.

and the nitrile group were involved in the binding interactions as H-bond acceptors with Lys-B352 and Lys-B254 amino acids, respectively.

ADME Predictions. The absorption, distribution, metabolism, and excretion (ADME) properties of compound 3b were predicted by the SwissADME free web tool (<http://www.swissadme.ch/index.php>). The studied compound showed a good oral bioavailability profile, which is clear through the bioavailability radar chart (Figure 14).

Moreover, it exhibited suitable physicochemical properties (Table 8), which was tested through the following six

Table 7. Docking Results of 3b in the Colchicine Binding Site of the Tubulin (TUB) Domain

compound	S (kcal/mol)	amino acids	interacting groups	type of interaction	length
3b	-11.3097	Ala-A180	O (C=O)	H-bond acceptor	3.26
		Val-A181	O (C=O)	H-bond acceptor	3.75
		Lys-B352	O (C=O)	H-bond acceptor	3.23
		Lys-B352	S	H-bond acceptor	3.51
		Lys-B254	N (CN)	H-bond acceptor	4.04

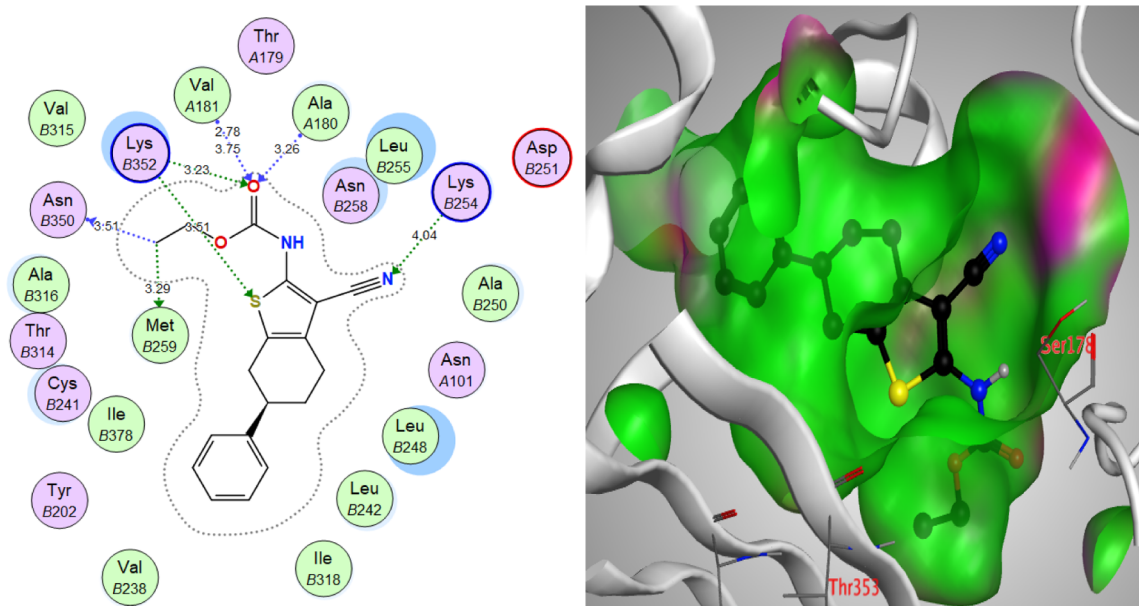


Figure 13. 2D and 3D interactions of compound 3b within the TUB active site.

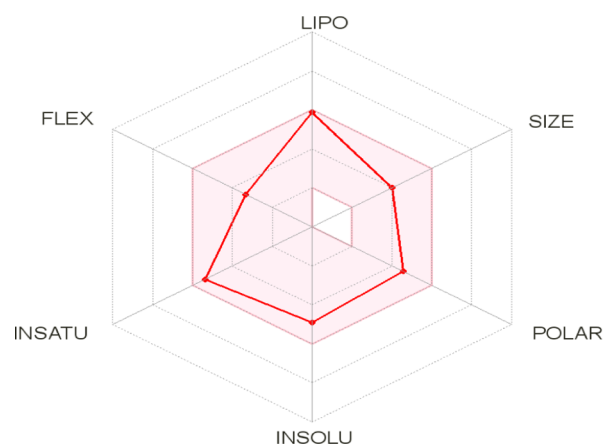


Figure 14. Bioavailability radar chart for compound 3b.

Table 8. Measured Physicochemical Parameters for Compound 3b

no. of heavy atoms	23
C-sp ³ fraction	0.33
no. of rotatable bonds	5
molar refractivity	91.55
topological polar surface area (TPSA)	90.36 Å ²
consensus log P _{o/w}	3.90

parameters: lipophilicity (LIPO), size, polarity (POLAR), insolubility (INSOL), unsaturation (UNSAT), and flexibility (FLEX). Concerning the absorption property, compound 3b showed high gastrointestinal tract (GIT) absorption as it is

located in the BOILED-EGG chart white area, indicating that it can be passively absorbed through the intestinal tract.

On the other hand, it is not expected to penetrate the blood brain barrier (located outside the chart yellow area). Moreover, it is not a potential substrate for permeability glycoprotein efflux protein (PGP), which is indicated by red, given for the tested compound (Figure 15).

Finally, compound 3b showed no violation to Lipinski's rule of five⁵⁵ as shown from data in Table 9.

Collectively, 3b possesses desirable drug-likeness and oral bioavailability properties.

CONCLUSIONS

A series of 4,5,6,7-tetrahydrobenzo[b]thiophene-conjugated amides, acetamides, carbamates, a cyclic imide and a Schiff base in addition to two Fe₃O₄-NPs were synthesized and characterized. These compounds were evaluated *in vitro* as inhibitors to the protumorigenic enzymes PDK-1 and LDHA, antioxidants, antibacterial, and anti-CRC agents on HCT-116 and LoVo cells. Although compound 1b showed promising enzymatic inhibitions and antioxidant potential, it failed to produce significant cytotoxic effects on the tested cell lines; probably, it may be selective toward other cell lines. The Schiff base derivative 11 did not display significant bioactivity. Contrarily, its modified Fe₃O₄ (12a) and Fe₃O₄/SiO₂ (12b) nanoparticles exhibited enhanced antioxidant, antibacterial, and cytotoxic activities with NPs 12a being the most active agent. Thus, the obtained data support further development of Fe₃O₄-NPs capped with Schiff bases derived from 3-substituted-2-amino-6-phenyl-4,5,6,7-tetrahydrobenzo[b]-

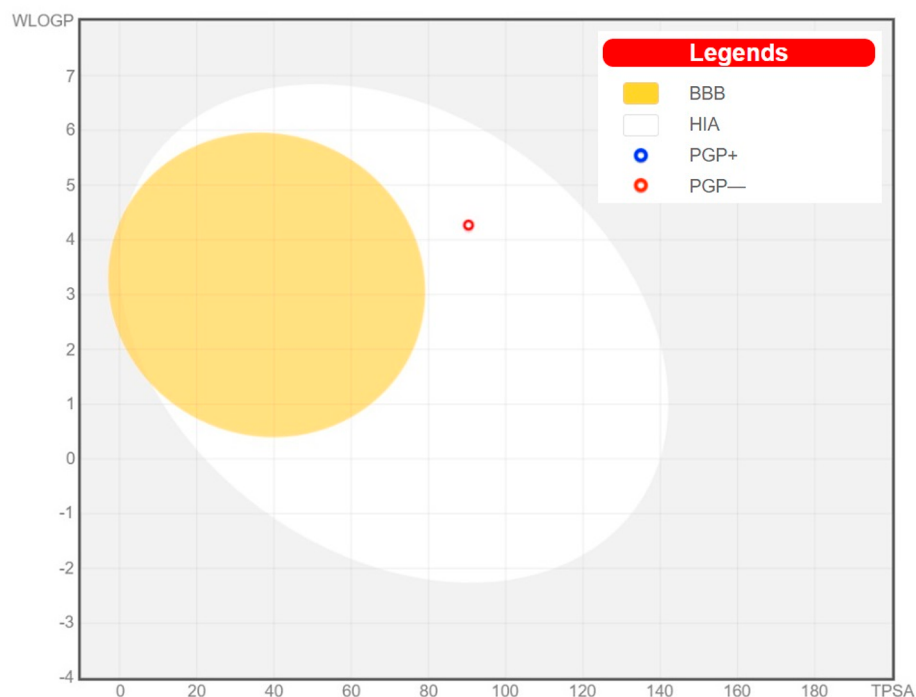


Figure 15. BOILED-EGG chart for compound 3b.

Table 9. Compliance of Compound 3b to Lipinski's Rule of Five

log $P = 3.90$	no violation as it is <5
molecular weight = 326.41 g/mol	no violation as it is <500
no. of H-bond donor groups (OHs + NHs) = 1	no violation as it is <5
no. of H-bond acceptor atoms (Os + Ns) = 4	no violation as it is <10

thiophene as potential CRC agents. Moreover, carbamate **3b** significantly inhibited the growth of both types of the examined colorectal cancerous cells. Thus, its capability to inhibit tubulin polymerization was investigated using molecular modeling analyses in addition to its ADME characteristics were predicted. The results of these analyses showed that **3b** exhibited reasonable affinity to the colchicine site of the tubulin (TUB) domain. It is involved in hydrogen bond interactions through sulfur atom, as well as nitrile and carbonyl groups with the amino acid residues in the binding site, implying that carbamate **3b** may induce antitumor effects on HCT-116 and LoVo cells via targeting tubulin polymerization. Furthermore, this 4,5,6,7-tetrahydrobenzo[*b*]thiophene derivative complied with Lipinski's rule of five; thus, it is expected to show good *in vivo* oral absorption. In addition, it possesses a desirable pharmacokinetic profile, which makes it an interesting structural template for the development of new antimitotic agents against CRC.

EXPERIMENTAL SECTION

Chemistry. General Information. The reactions were monitored, and the purity of the final products was checked using TLC analysis on pre-coated silica gel sheets (60 F254, Merck, and Kenilworth, NJ). The developed plates were examined by exposure to ultraviolet light using a VL-6.LC (254, 365 nm, 50/60 Hz). All the melting points were determined in open capillary tubes with a Gallenkamp melting point apparatus ($^{\circ}\text{C}$). The IR spectra were recorded on a

PerkinElmer Fourier transform infra-red (FTIR) spectrophotometer (Spectrum BX 1000) in wave numbers (cm^{-1}) with potassium bromide (KBr) discs. Nuclear magnetic resonance (NMR) spectra were recorded on an Eclipse 300 FT NMR spectrometer operating at 300 MHz for ^1H and at 75 MHz for ^{13}C at 25 $^{\circ}\text{C}$ (KSU, Riyadh, KSA). The chemical shifts (δ) were expressed in ppm using tetramethylsilane as the internal standard; coupling constants (J) were expressed in Hz. Mass spectra were recorded on a Shimadzu Qp-2010 Plus mass spectrometer in the ionization mode: EI (Regional Center for Mycology and Biotechnology, Al-Azhar University, Egypt).

The physical and spectroscopic data of compounds **1a-c**^{56,57} and **3c**⁵⁸ are consistent with those previously reported.

Synthesis of Carbamate Derivatives (3a,b). A mixture of aminothiophene **1a** or **1b** (0.0028 mol) and ethyl chloroformate **2a** (0.038 mol) was refluxed for 10 h. The excess reagent was evaporated under reduced pressure; the remaining residue was treated with diethyl ether, and the precipitated solid was filtered off, washed with water, air-dried, and purified by recrystallization from benzene to give carbamates **3a,b**, respectively.

Ethyl 2-((Ethoxycarbonyl)amino)-6-phenyl-4,5,6,7-tetrahydrobenzo[*b*]thiophene-3-carboxylate (3a). Buff powder; R_f : 0.88 (petroleum ether/ethyl acetate, 1:2); yield (86%); mp 107–109 $^{\circ}\text{C}$; IR (KBr) $\nu_{\text{max}}/\text{cm}^{-1}$: 3251 (NH), 3020 (CH-Ar), 2983, 2929 (CH-aliphatic), 1725, 1652 ($2 \times \text{C}=\text{O}$), 1434, 1236, 1058, 846, 763, 697, 542; ^1H NMR (300 MHz, DMSO- d_6): δ_{H} 1.22 (t, 6H, $J = 6.9$ Hz, $2 \times \text{CH}_3$), 1.75–1.95 (m, 2H, CH_2), 2.58–2.88 (m, 5H, $2 \times \text{CH}_2$, CH), 4.20 (q, 4H, $J = 7.2$ Hz, $2 \times \text{CH}_2\text{O}$), 7.17–7.26 (m, 5H, $5 \times \text{Ar-H}$), 10.33 (s, 1H, NH); ^{13}C NMR (75 MHz, DMSO- d_6): δ_{C} 13.92, 14.12 (CH_3), 26.27, 29.54, 30.57, 31.34 ($3 \times \text{CH}_2$, CH), 60.29, 61.99 ($2 \times \text{OCH}_2$), 110.12, 124.72, 126.14, 126.67, 128.27, 130.44, 145.55, 148.46, 152.13, 165.21 ($5 \times \text{CH-Ar}$, $5 \times \text{C}_q\text{-Ar}$ & $2 \times \text{C}=\text{O}$); MS (EI, 70 eV) m/z (%): 376.27 [$\text{M}^+ + 3$, 23] and 375.41 [$\text{M}^+ + 2$, 32] for $\text{C}_{20}\text{H}_{23}\text{NO}_4\text{S}$, 366.64

(61), 343.07 (31), 329.98 (65), 328.97 (61), 321.08 (56), 296.61 (45), 277.34 (35), 230.48 (35), 190.70 (37), 177.89 (55), 173.89 (100), 155.22 (65), 134.01 (61), 125.66 (81), 89.03 (50), 52.57 (50).

Ethyl (3-Cyano-6-phenyl-4,5,6,7-tetrahydrobenzo[b]thiophen-2-yl)carbamate (3b). Buff powder; R_f : 0.89 (petroleum ether/ethyl acetate, 1:1); yield (80%); mp 177–178 °C; IR (KBr) $\nu_{\max}/\text{cm}^{-1}$: 3221 (NH), 3098 (CH-Ar), 2988, 2926 (CH-aliphatic), 2219 (CN), 1725 (C=O), 1465, 1236, 1069, 882, 761, 699, 547; ^1H NMR (300 MHz, DMSO- d_6): δ_{H} 1.22 (t, 3H, $J = 7.1$ Hz, CH₃), 1.87–1.97 (m, 2H, CH₂), 2.61–2.97 (m, 5H, CH, 2 × CH₂), 4.21 (q, 2H, $J = 7.1$ Hz, CH₂O), 7.22–7.30 (m, 5H, 5 × Ar-H), 11.18 (s, 1H, NH); ^{13}C NMR (75 MHz, DMSO- d_6): δ_{C} 14.31 (CH₃), 24.13, 29.00, 31.25 (3 × CH₂, CH), 61.78 (OCH₂), 93.90, 113.98, 126.34, 126.86, 128.41, 128.73, 131.18, 133.07, 145.38, 148.55, 153.57 (5 × CH-Ar, 5 × C_q-Ar, CN & C=O); MS (EI, 70 eV) m/z (%): 328.41 [$M^+ + 2$, 26] for C₁₈H₁₈N₂O₂S, 320.29 (47), 316.67 (97), 285.67 (50), 284.40 (41), 272.55 (31), 253.21 (60), 241.01 (52), 229.56 (36), 192.02 (66), 186.39 (54), 170.74 (32), 140.77 (30), 123.84 (100), 85.28 (32), 77.22 (76), 63.22 (50).

Synthesis of Amide Derivatives (3c–f). To a solution of compound **1a** or **1b** (0.02 mol) in CHCl₃ (30 mL) containing triethylamine (0.024 mol), the appropriate acid chloride (0.024 mol): chloroacetyl chloride **2b**, thiophene-2-carbonyl chloride **2c**, or 4-chlorobenzoyl chloride **2d**, was added drop wise at 0 °C and the resulting reaction mixture in each case was stirred at r.t for 1 h then refluxed for 16 h. Evaporation of the solvent and treatment of the remaining residue with soln. of NaHCO₃ gave the crude product, which was collected by filtration, and air dried. Recrystallization from ethanol gave the pure amides, the previously reported **3c**⁴¹ and the new derivatives **3d–g**, respectively.

2-Chloro-N-(3-cyano-6-phenyl-4,5,6,7-tetrahydrobenzo[b]thiophen-2-yl) Acetamide (3d). Brown crystal; R_f : 0.82 (petroleum ether/ethyl acetate, 1:1); yield (70%); mp 170–172 °C; IR (KBr) $\nu_{\max}/\text{cm}^{-1}$: 3239 (NH), 3089 (CH), 2980, 2940 (CH₂), 2208 (CN), 1708 (C=O), 1479, 1176, 1034, 806, 694, 536; ^1H NMR (300 MHz, DMSO- d_6): δ_{H} 1.90–2.00 (m, 2H, CH₂), 2.65–3.06 (m, 5H, 2 × CH₂, CH), 4.48 (s, 2H, CH₂-CO), 7.21–7.39 (m, 5H, 5 × Ar-H), 10.59 (s, 1H, NH); ^{13}C NMR (75 MHz, DMSO- d_6): δ_{C} 23.98, 28.98, 31.12, 42.28, 45.34 (3 × CH₂, CH, CH₂-CO), 93.38, 113.99, 126.33, 126.84, 127.64, 128.41, 130.83, 145.30, 146.17 (5 × CH-Ar, 5 × C_q-Ar & CN), 164.64 (C=O); MS (EI, 70 eV) m/z (%): 332.82 [$M^+ + 2$, 4] for C₁₇H₁₅ClN₂OS, 328.17 (8), 315.13 (30), 253.17 (30), 181.26 (100), 163.09 (23), 153.07 (50), 119.24 (23), 101.37 (28), 91.05 (46), 89.26 (27).

Ethyl 6-Phenyl-2-(thiophene-2-carboxamido)-4,5,6,7-tetrahydrobenzo[b] thiophene-3-carboxylate (3e). Pale yellow powder; R_f : 0.76 (petroleum ether/ethyl acetate, 1:2); yield (60%); mp 185–187 °C; IR (KBr) $\nu_{\max}/\text{cm}^{-1}$: 3233 (NH), 3095 (CH-Ar), 2928 (CH-aliphatic), 1718, 1646 (2 × C=O), 1412, 1219, 1025, 841, 729, 694, 538; ^1H NMR (300 MHz, CDCl₃): δ_{H} 1.36 (t, 3H, $J = 6.9$ Hz, CH₃), 1.80–2.12 (m, 2H, CH₂), 2.70–2.99 (m, 5H, 2 × CH₂, CH), 4.34 (q, 2H, $J = 7.2$ Hz, CH₂O), 7.08–7.11 (m, 1H, Ar-H), 7.19–7.31 (m, 5H, 5 × Ar-H), 7.54 (dd, 1H, $J = 3.6, 1.2$ Hz, Ar-H), 7.71 (dd, 1H, $J = 2.4, 1.2$ Hz, Ar-H), 12.13 (s, 1H, NH-C=O); ^{13}C NMR (75 MHz, CDCl₃): δ_{C} 11.21 (CH₃), 23.59, 26.96, 29.03, 37.38 (3 × CH₂, CH), 57.54 (CH₂O), 108.42, 123.22, 123.44, 123.70, 124.90, 125.35, 126.12, 127.64, 128.66, 134.50, 142.60,

144.83, 155.08, 163.63 (8 × CH-Ar, 6 × C_q-Ar & 2 × C=O); MS (EI, 70 eV) m/z (%): 415.68 [$M^+ + 4$, 8] for C₂₂H₂₁NO₃S₂, 414.27 (19), 373.12 (40), 357.50 (48), 350.06 (46), 330.06 (33), 296.42 (79), 292.80 (36), 269.46 (84), 268.30 (100), 253.11 (69), 239.41 (30), 224.29 (47), 176.90 (38), 163.16 (56), 149.29 (79), 135.21 (33), 119.15 (32), 106.85 (49), 93.55 (60), 90.36 (50), 77.09 (94), 65.46 (83), 41.13 (59).

4-Chloro-N-(3-cyano-6-phenyl-4,5,6,7-tetrahydrobenzo[b]thiophen-2-yl) Benzamide (3f). Brown powder; R_f : 0.91 (petroleum ether/ethyl acetate, 1:1); yield (60%); mp 205–207 °C; IR (KBr) $\nu_{\max}/\text{cm}^{-1}$: 3246 (NH), 3079 (CH-Ar), 2978, 2930 (CH-aliphatic), 2218 (CN), 1663 (C=O), 1481, 1276, 1089, 846, 750, 695, 534; ^1H NMR (300 MHz, DMSO- d_6): δ_{H} 1.87–1.99 (m, 2H, CH₂), 2.65–2.75 (m, 2H, CH₂), 2.87–3.05 (m, 3H, CH₂, CH), 7.20–7.30 (m, 5H, 5 × Ar-H), 7.61 (d, 2H, $J = 8.4$ Hz, 2 × Ar-H), 8.00 (d, 2H, $J = 8.4$ Hz, 2 × Ar-H), 10.90 (s, 1H, NH-C=O); ^{13}C NMR (75 MHz, DMSO- d_6): δ_{C} 24.09, 29.03, 31.23, 45.31 (3 × CH₂, CH), 95.85, 114.16, 126.32, 126.83, 128.40, 128.51, 128.67, 128.85, 130.27, 131.11, 137.20, 145.31, 146.44, 164.15 (9 × CH-Ar, 7 × C_q-Ar, CN & C=O); MS (EI, 70 eV) m/z (%): 396.05 [$M^+ + 4$, 17] for C₂₂H₁₇ClN₂OS, 395.34 (6), 392.00 (11), 390.79 (7), 389.51 (6), 388.86 (5), 384.50 (100), 372.20 (40), 357.81 (44), 341.13 (40), 304.04 (36), 254.82 (36), 240.84 (39), 178.47 (41), 157.43 (33), 116.94 (36), 102.50 (32), 91.56 (45), 78.24 (47), 65.22 (79), 51.70 (51).

General Procedures for Condensation of Chloroacetamides 3c,d with 2° Amines. A mixture of chloroacetamide derivative **3c** or **3d** (0.025 mol) and 0.03 mol of morpholine **4a** or 1-(pyridin-2-yl)piperazine **4b** in CH₃OH (30 mL) was refluxed for 10 h. The excess solvent was evaporated, and the remaining residue was treated with cold water. The obtained solid product in each case was collected by filtration, air-dried, and recrystallized from ethanol to give compounds **5a–c**, respectively.

Ethyl 2-(2-Morpholinoacetamido)-6-phenyl-4,5,6,7-tetrahydrobenzo[b]thiophene-3-carboxylate (5a). Beige powder; R_f : 0.32 (petroleum ether/ethyl acetate, 1:2); yield (55%); mp 90–93 °C; IR (KBr) $\nu_{\max}/\text{cm}^{-1}$: 3233 (NH), 2926 (CH₂), 1728, 1671 (2 × C=O), 1440, 1232, 1035, 866, 754, 699, 542; ^1H NMR (300 MHz, DMSO- d_6): δ_{H} 1.31 (t, 3H, $J = 6.9$ Hz, CH₃), 1.84–2.08 (m, 2H, CH₂), 2.51 (apparent s, 4H, 2 × CH₂N), 2.64–2.92 (m, 5H, 2 × CH₂, CH), 3.24 (s, 2H, CH₂-CO), 3.69 (apparent s, 4H, 2 × CH₂O), 4.32 (q, 2H, $J = 7.2$ Hz, CH₂O), 7.20–7.28 (m, 5H, 5 × Ar-H), 12.13 (s, 1H, NH); ^{13}C NMR (75 MHz, DMSO- d_6): δ_{C} 14.14 (CH₃), 26.30, 29.69, 31.43 (3 × CH₂, CH), 53.21, 60.24, 60.58, 66.15 (4 × CH₂-morpholine ring, OCH₂-ester, CH₂-N), 111.22, 125.51, 126.18, 126.75, 128.32, 130.13, 145.62, 146.05, 164.83, 167.78 (5 × CH-Ar, 5 × C_q-Ar, 2 × C=O); MS (EI, 70 eV) m/z (%): 431.13 [$M^+ + 3$, 25] and 430.23 [$M^+ + 2$, 11] for C₂₃H₂₈N₂O₄S, 424.00 (10), 361.40 (26), 340.69 (31), 308.89 (27), 273.95 (31), 263.09 (37), 231.37 (29), 224.28 (45), 211.28 (39), 185.48 (70), 151.55 (100), 147.35 (55), 143.11 (63), 134.15 (31), 116.12 (70), 114.83 (79), 101.95 (93), 78.48 (52), 64.66 (57), 44.12 (95).

Ethyl-6-phenyl-2-(2-(4-(pyridin-2-yl)piperazin-1-yl)-acetamido)-4,5,6,7-tetrahydro Benzo[b]thiophene-3-carboxylate (5b). Beige powder; R_f : 0.32 (petroleum ether/ethyl acetate, 1:2); yield (70%); mp 189–191 °C; IR (KBr) $\nu_{\max}/\text{cm}^{-1}$: 3222 (NH), 3042 (CH-Ar), 2983, 2941, 2910 (CH-aliphatic), 1724, 1662 (2 × C=O), 1597 (C=N), 1522

(C=C), 1436, 1237, 1014, 772, 696, 541; ^1H NMR (300 MHz, DMSO- d_6): δ_{H} 1.29 (t, 3H, $J = 6.9$ Hz, CH_3), 1.82–2.08 (m, 2H, CH_2), 2.46–3.04 (m, 9H, $2 \times \text{CH}_2$ and CH-cyclohexene, $2 \times \text{CH}_2\text{N}$), 3.43 (s, 2H, $\text{CH}_2\text{-CO}$), 3.60 (apparent s, 4H, $2 \times \text{CH}_2\text{N}$), 4.27 (q, 2H, $J = 7.2$ Hz, CH_2O), 6.60–6.70 (m, 1H, CH-pyridine), 6.84 (d, 1H, $J = 8.1$ Hz, CH-pyridine), 7.18–7.31 (m, 5H, $5 \times \text{CH-Ph}$), 7.56 (apparent td, 1H, $J = 8.1, 2.4$ Hz, CH-pyridine), 8.10–8.20 (m, 1H, CH-pyridine), 12.16 (s, 1H, NH); ^{13}C NMR (75 MHz, DMSO- d_6): δ_{C} 14.14 (CH_3), 26.32, 29.72, 31.46 ($3 \times \text{CH}_2$ and CH of the cyclohexene ring), 45.00, 52.62 ($\text{C-CH}_2\text{C=O}$ and $4 \times \text{CH}_2$ -piperazine ring), 60.29 (CH_2 -ester), 107.16, 111.30, 113.11, 125.61, 126.24, 126.83, 128.37, 130.22, 137.56, 145.67, 146.06, 147.57, 158.92, 164.86, 167.95 ($9 \times \text{CH-Ar}$, $6 \times \text{C}_q\text{-Ar}$, $2 \times \text{C=O}$); MS (EI, 70 eV) m/z (%): 506.41 [$\text{M}^+ + 2$, 24] for $\text{C}_{28}\text{H}_{32}\text{N}_4\text{O}_3\text{S}$, 505.86 (24), 453.56 (50), 451.55 (48), 422.36 (40), 369.47 (100), 338.04 (59), 325.11 (50), 300.70 (47), 293.04 (76), 280.27 (76), 174.82 (56), 165.63 (45), 71.68 (46), 54.45 (82).

***N*-(3-Cyano-6-phenyl-4,5,6,7-tetrahydrobenzo[*b*]thiophen-2-yl)-2-morpholino Acetamide (5c).** Dark brown powder; yield (58%); mp 182–185 °C; IR (KBr) $\nu_{\text{max}}/\text{cm}^{-1}$: 3428 (NH), 2924, 2852 (CH-aliphatic), 2205 (CN), 1679 (C=O), 1446, 1229, 1039, 870, 754, 698, 515; MS (EI, 70 eV) m/z (%): 383.60 [$\text{M}^+ + 2$, 11] for $\text{C}_{21}\text{H}_{23}\text{N}_3\text{O}_2\text{S}$, 382.81 (30), 381.45 (10), 379.07 (24), 371.66 (56), 341.76 (81), 317.82 (62), 283.91 (39), 281.04 (76), 279.77 (88), 244.76 (45), 218.42 (77), 205.23 (63), 197.82 (59), 173.35 (100), 133.29 (63), 97.00 (73), 91.16 (93), 81.14 (75), 74.10 (78), 63.35 (77), 44.12 (70).

Synthesis of 2-(2,5-Dioxopyrrolidin-1-yl)-6-phenyl-4,5,6,7-tetrahydrobenzo[*b*]thiophene-3-carbonitrile (7). Equimolar amounts (5 mmol) of aminothiophene **1b** and succinic anhydride **6** in the presence of freshly fused sodium acetate (5 mmol) were fused in an oil bath for 2 h. After cooling to r.t., the reaction mixture was treated with conc. HCl (37.5%, 2 mL). The separated solid was filtered off, washed with water, air-dried, and recrystallized from ethanol to yield the *title compound* as a yellow powder; R_f : 0.49 (petroleum ether/ethyl acetate, 1:1); yield (60%); mp 157–160 °C; IR (KBr) $\nu_{\text{max}}/\text{cm}^{-1}$: 3027 (CH-Ar), 2923 (CH-aliphatic), 2216 (CN), 1728, 1662 ($2 \times \text{C=O}$), 1495 (C=C), 1439, 1283, 1164, 912, 757, 700, 540; ^1H NMR (300 MHz, DMSO- d_6): δ_{H} 1.98–2.08 (m, 2H, CH_2), 2.75–3.08 (m, 9H, $4 \times \text{CH}_2$, CH), 7.21–7.32 (m, 5H, $5 \times \text{Ar-H}$); ^{13}C NMR (75 MHz, DMSO- d_6): δ_{C} 24.40, 25.76, 28.67, 28.90, 29.33, 31.90 ($5 \times \text{CH}_2$, CH), 107.55, 112.96, 126.44, 126.59, 127.00, 128.55, 128.62, 133.70, 136.70, 145.22, 145.70 ($5 \times \text{CH-Ar}$, $5 \times \text{C}_q\text{-Ar}$ and CN), 175.44 ($2 \times \text{CO}$); MS (EI, 70 eV) m/z (%): 338.32 [$\text{M}^+ + 2$, 26] for $\text{C}_{19}\text{H}_{16}\text{N}_2\text{O}_2\text{S}$, 336.64 (51), 315.16 (34), 281.54 (45), 258.21 (71), 243.27 (50), 231.75 (100), 220.56 (42), 158.80 (31), 119.22 (48), 45.82 (39).

Synthesis of *N'*-(3-Cyano-6-phenyl-4,5,6,7-tetrahydrobenzo[*b*]thiophen-2-yl)-*N,N*-dimethyl Formamidine (9). To a solution of aminothiophene **1b** (4 mmol) in dry xylene (15 mL), DMF–DMA **8** (4 mmol) was added. The reaction mixture was heated under reflux for 10 h. The separated solid was filtered off and recrystallized from EtOH to give the *title compound* as a buff powder; R_f : 0.67 (petroleum ether/ethyl acetate, 1:1); yield (70%); mp 120–122 °C; IR (KBr) $\nu_{\text{max}}/\text{cm}^{-1}$: 3027 (CH-Ar), 2920 (CH-aliphatic), 2205 (CN), 1628 (C=N), 1572, 1401, 1262, 972, 871, 758, 700, 546; ^1H NMR (300 MHz, DMSO- d_6): δ_{H} 1.74–1.97 (m, 2H, CH_2), 2.50–

2.80 (m, 5H, $2 \times \text{CH}_2$, CH), 2.98 (s, 3H, $\text{CH}_3\text{-N}$), 3.08 (s, 3H, $\text{CH}_3\text{-N}$), 7.21–7.31 (m, 5H, $5 \times \text{Ar-H}$), 7.96 (s, 1H, N=CH); ^{13}C NMR (75 MHz, DMSO- d_6): δ_{C} 24.46, 29.14, 32.12 ($3 \times \text{CH}_2$, CH), 34.62, 38.81 ($2 \times \text{CH}_3\text{-N}$), 95.48, 116.05, 122.97, 126.38, 126.93, 128.48, 131.93, 145.58, 155.28, 164.88 ($5 \times \text{CH-Ar}$, $5 \times \text{C}_q\text{-Ar}$, CN & CH=N); MS (EI, 70 eV) m/z (%): 311.49 [$\text{M}^+ + 2$, 57] for $\text{C}_{18}\text{H}_{19}\text{N}_3\text{S}$, 308.87 (14), 306.47 (64), 296.95 (39), 284.36 (32), 272.55 (74), 261.15 (42), 249.12 (45), 238.22 (55), 236.25 (64), 216.32 (60), 200.89 (68), 185.82 (39), 176.87 (47), 161.77 (53), 157.32 (73), 143.69 (81), 132.65 (61), 124.55 (82), 108.84 (59), 93.18 (100), 90.59 (92), 71.96 (44), 65.33 (59), 53.36 (78).

Synthesis of 2-((3-Hydroxy-4-methoxybenzylidene)-amino)-4,5,6,7-tetrahydrobenzo[*b*]thiophene-3-carbonitrile (11). To an equimolar (0.01 mol) solution of aminothiophene **1c** and isovanillin **10** in ethanol (30 mL), acetic acid (3 mL) was added. The resulting reaction mixture was refluxed for 12 h. Evaporation of the excess solvent gave the crude product, which was recrystallized from ethanol to give the *title compound* as a yellowish green powder; R_f : 0.79 (petroleum ether/ethyl acetate, 4:1); yield (80%); mp 190–192 °C; IR (KBr) $\nu_{\text{max}}/\text{cm}^{-1}$: 3403 (OH), 3027 (CH-Ar), 2931 (CH-aliphatic), 2220 (CN), 1595 (C=N); 1521 (C=C), 1440, 1281, 1018, 895, 795, 699, 540; ^1H NMR (300 MHz, DMSO- d_6): δ_{H} 1.73 (apparent s, 4H, $2 \times \text{CH}_2$), 2.06 (apparent s, 2H, CH_2), 2.60 (apparent s, 2H, CH_2), 3.83 (s, 3H, OCH_3), 7.02 (d, 1H, $J = 8$ Hz, Ar-H), 7.31 (dd, 1H, $J = 6.4, 1.6$ Hz, Ar-H), 7.47 (s, 1H, Ar-H), 8.36 (s, 1H, CH=N), 9.52 (s, 1H, OH); ^{13}C NMR (75 MHz, DMSO- d_6): δ_{C} 21.61, 22.40, 23.72, 24.49 ($4 \times \text{CH}_2$), 55.65 (OCH_3), 104.87, 111.43, 113.43, 114.43, 124.31, 127.79, 131.59, 134.00 ($3 \times \text{CH-Ar}$, $4 \times \text{C}_q\text{-Ar}$ & CN), 147.06, 152.22, 159.90, 160.43 ($2 \times \text{C}_q\text{-O}$, $\text{S-C}_q\text{-N}$ & HC=N); MS (EI, 70 eV) m/z (%): 315.74 [$\text{M}^+ + 3$, 4] and 314.82 [$\text{M}^+ + 2$, 10] for $\text{C}_{17}\text{H}_{16}\text{N}_2\text{O}_2\text{S}$, 313.55 (16), 312.34 (10), 213.66 (56), 201.35 (42), 105.26 (59), 77.13 (100), 74.39 (53), 69.91 (58), 64.21 (77), 50.30 (39).

Synthesis of Magnetite and Magnetic Silicate NPs Supported with the 4,5,6,7-Tetrahydrobenzo[*b*]thiophene-3-carbonitrile Schiff Base Derivative (11).

Synthesis of Fe_3O_4 NPs by the Co-precipitation Method. 500 mL of 1.5 M NaOH was added dropwise with continuous stirring for 4 h at 80 °C to a mixture of (0.04 mol, 10.8 g) $\text{FeCl}_3 \cdot 6\text{H}_2\text{O}$ and (0.02 mol, 5.5 g) $\text{FeSO}_4 \cdot 7\text{H}_2\text{O}$ dissolved in 50 mL of 0.5 M HCl. The result Fe_3O_4 precipitant was separated with a magnet and washed a few times with deionized water and dried at 50 °C for 7 h.

Modification of the Surface of Fe_3O_4 NPs by 2-((3-Hydroxy-4-methoxy benzylidene)amino)-4,5,6,7-tetrahydrobenzo[*b*]thiophene-3-carbonitrile (12a). A solution of Fe_3O_4 NPs (0.8 g) and compound **11** (0.4 g) in a mixture of EtOH/ H_2O (70:30) were stirred for 4 h at 70 °C. The resulting Fe_3O_4 was collected with an external magnet, washed several times with ethanol, and dried at room temperature.

Synthesis of Silica-Coated Fe_3O_4 Nanomolecules (12b). The coated Fe_3O_4 NPs (**12a**, 0.5 g) were dispersed under sonication for 30 min in a mixture of deionized H_2O /EtOH/ NH_3 (10:30:10) v/v. TEOS (2.5 mL) was added dropwise to the magnetite colloid under mechanical stirring for 22 h. The prepared $\text{Fe}_3\text{O}_4/\text{SiO}_2$ nanocomposite was separated using an external magnet, washed several times with distilled H_2O and dried at room temperature.

Biological Screening. Enzymatic Inhibitory Assays. Pyruvate Dehydrogenase Kinase (PDK1) Activity Assay. A

Kinase-Glo Luminescent Kinase kit was used to determine the PDK-1 activities. Briefly, 5 μL of the assay buffer (10 \times 250 mM Tris-HCl, 50 mM MgCl_2 , 5 mM EGTA, 10 mM EDTA, and 10 mM DTT) and 25 μL of distilled water were added to a 96-well plate. After that, different concentrations (25, 50, 75, 100, 200, and 300 μg) of each tested compound (5 μL) were added to each well, except for the two control wells containing 5 μL of PBS buffer or 1% DMSO. Then, 5 μL of PDH E1 protein (10 μM) and 5 μL of ATP (10 μM) were added to all the wells. Subsequently, 5 μL of PDK-1 (20 μM) in protein buffer (1 mM MgCl_2 , 2000 mM KCl, 40 mM K_3PO_4) was added to all the wells, while 5 μL of protein buffer was added to the control wells. Thereafter, the plate was well mixed and incubated for 30 min at 37 $^\circ\text{C}$. Then, 50 μL of the appropriate kinase-Glo reagent was added to each well. Finally, the plate was incubated at room temperature for 10 min under gentle shaking, and then, the luminescence was recorded on a Microplate Reader. Sodium dichloroacetate (1000 μM) was used as the standard drug for inhibition of PDK1.

Lactate Dehydrogenase (LDH) Inhibition Assay. LDHA inhibition activity was investigated by measuring the amounts of consumed NADH.⁵⁹ Briefly, different concentrations of each compound (25, 50, 75, 100, 200, and 300 μg) were incubated in a buffer containing 20 mM of HEPES-K+ (pH 7.2), 20 μM of NADH, 2 mM of pyruvate, and 10 ng of purified recombinant human LDHA protein for 10 min. The fluorescence of NADH, which has an excitation wavelength of 340 nm and an emission wavelength of 460 nm, was detected using a spectrofluorometer. Sodium oxamate (1000 μM) was used as a standard inhibitor for LDHA.

DPPH Radical Scavenging Effect. The 1,1-diphenyl-2-picrylhydrazyl (DPPH) radical scavenging method was used to investigate the antioxidant potency of the all studied compounds.⁶⁰ Briefly, a 0.5 mL volume of DPPH ethanolic solution was mixed with an equal volume of each sample concentration, shaken strongly, and incubated at room temperature for 1 h in darkness. The absorbance of the residual DPPH radicals was measured at 519 nm and compared to the control (without the tested compound), while BHT was used as a positive control. The DPPH radical scavenging potency was calculated using the following formula:

$$\text{scavenging effect (\%)} = (1 - A_{\text{compound}}/A_{\text{control}}) \times 100$$

where A_{compound} and A_{control} are the absorbances of the tested compound and the control, respectively. The plot of the scavenging effect (%) versus the compound concentration was also performed to determine the compound concentration providing 50% inhibition (IC_{50}).

Antibacterial Assay. Pure standard microbial isolates collected from King Khaled University Hospital were tested in this study, including *E. faecalis* (ATCC: 29122) as Gram-positive bacteria and *E. coli* (ATCC: 25922) as Gram-negative bacteria. Fresh cultures of each microorganism were grown on nutrient agar plates (Oxoid, UK), of which small inoculums were suspended in 5 mL nutrient broth for bacterial suspension preparation of 0.5 MacFarland. Bacterial viability was investigated by determining the colony-forming ability (CFU) of bacteria incubated at different time intervals without or with appropriate amounts of the compound that were mixed with 2×10^7 CFU/mL in sterile BHI and were incubated under shaking for 60 min at 37 $^\circ\text{C}$. Samples were serially diluted into sterile BHI, streaked onto media agar plates, and

incubated for 24 h at 37 $^\circ\text{C}$. The antibacterial potency of each tested compound was expressed as the residual number of CFU with reference to the initial inoculums. The results presented as the half-maximal (50%) inhibitory concentration (IC_{50}) are means of two different measurements. Ampicillin was used as a positive standard reference.

Cytotoxicity Assays on HCT-116 and LoVo Human CRC Cells. Cytotoxic potency was examined on human CRC cell lines HCT-116 and LoVo (American Type Culture Collection; USA) using various amounts of tested compounds (25, 50, 75, 100, 200, and 400 μg). Samples were diluted in Dulbecco's modified Eagle's medium, consisting of 10% fetal bovine serum, added to cells grown and cultured for 24 h in a 5% CO_2 -humidified incubator at 37 $^\circ\text{C}$. Then, the activity of lactate dehydrogenase released from damaged cells was determined in the collected supernatant aliquots using an ELISA end-point assay (Benchmark Plus, Bio-Rad, CA, USA). 0.1% Triton X-100 in the assay medium and the assay medium only were used as positive and negative controls, respectively. Cell viability, expressed as a relative percentage of the OD (optical density) values (at 550 nm) for compound-treated cells (a final concentration of 100 μg) and the control, is shown as the mean \pm SD ($n = 2$). The plot of the cell viability (%) versus the compound's concentration was also performed to determine the compound's concentration providing 50% inhibition (IC_{50}).

Molecular Docking. All the molecular modeling studies were carried out using Molecular Operating Environment (MOE, 2019.0102) software. All minimizations were performed with MOE until an RMSD gradient of $0.1 \text{ kcal}\cdot\text{mol}^{-1} \text{ \AA}^{-1}$ with the MMFF94x force field, and the partial charges were automatically calculated. The X-ray crystallographic structure of the tubulin (TUB) domain complexed with colchicine (COL) (PDB ID: 5NMS) was downloaded from the protein data bank (<https://www.rcsb.org/structure/5NMS>). For the co-crystallized enzyme, water molecules and ligands, which are not involved in the binding, were removed, and the protein was prepared for the docking study using the Protonate 3D protocol in MOE with default options. The co-crystallized ligand (COL) was used to define the binding site for docking. The Triangle Matcher placement method and London dG scoring function were used for docking.

ADME Profiling. The ADME properties of compound **3b** were studied by the SwissADME free web tool (<http://www.swissadme.ch/index.php>), accessed on 26 July 2021.

AUTHOR INFORMATION

Corresponding Author

Nahed Nasser Eid El-Sayed – National Organization for Drug Control and Research, Egyptian Drug Authority, Giza 35521, Egypt; orcid.org/0000-0001-9771-8956; Email: nahed.elsayed@edaegypt.gov.eg, nnelsayed@gmail.com

Authors

Shimaa Kamal – Chemistry Department, Faculty of Science, Ain Shams University, Cairo 11566, Egypt
Hamed Ahmed Derbala – Chemistry Department, Faculty of Science, Ain Shams University, Cairo 11566, Egypt
Seham Soliman Alterary – Department of Chemistry, College of Science, King Saud University, Riyadh 11523, Saudi Arabia; orcid.org/0000-0002-4176-2840

Abir Ben Bacha – Biochemistry Department, College of Science, King Saud University, Riyadh 11495, Saudi Arabia

Mona Alonazi – Biochemistry Department, College of Science, King Saud University, Riyadh 11495, Saudi Arabia

Mohamed Kandeel El-Ashrey – Pharmaceutical Chemistry Department, Molecular Modeling Unit, Faculty of Pharmacy, Cairo University, Cairo 11562, Egypt; Present

Address: Medicinal Chemistry Department, Faculty of Pharmacy, King Salman International University, Ras-Sedr, South Sinai, Egypt; orcid.org/0000-0002-3548-3888

Complete contact information is available at:

<https://pubs.acs.org/10.1021/acsofd.1c04063>

Author Contributions

S.K. performed the chemistry experiments, interpreted chemistry data, and wrote the original draft of the manuscript. N.N.E.E.-S. designed the work, interpreted chemistry data with S.K. and all the biological results, supervised the student, and rewrote the manuscript as is in the final form. H.A.D. reviewed and edited the manuscript. S.S.A. secured a place for the student at KSU, designed the Nano experiments, helped with morphological characterization of NPs, and provided with N.N.E.E.-S. all chemicals. A.B.B. and M.A. performed biological activity and fund acquisition. M.K.E.-A. performed and interpreted the docking and ADME analyses.

Notes

The authors declare no competing financial interest.

ACKNOWLEDGMENTS

The authors acknowledge Researchers Supporting Project number RSP-2021/237, King Saud University, Riyadh, Saudi Arabia.

REFERENCES

- (1) Keum, N.; Giovannucci, E. Global burden of colorectal cancer: emerging trends, risk factors and prevention strategies. *Nat. Clin. Pract. Gastroenterol. Hepatol.* **2019**, *16*, 713–732.
- (2) Al-Zalabani, A. Preventability of colorectal cancer in Saudi Arabia: fraction of cases attributable to modifiable risk factors in 2015–2040. *Int. J. Environ. Res. Public Health* **2020**, *17*, 320–340.
- (3) Wright, M.; Beaty, J. S.; Ternent, C. A. Molecular markers for colorectal cancer. *Surg. Clin.* **2017**, *97*, 683–701.
- (4) Collins, D.; Hogan, A. M.; Winter, D. C. Microbial and viral pathogens in colorectal cancer. *Lancet Oncol.* **2011**, *12*, 504–512.
- (5) Geravand, M.; Fallah, P.; Yaghoobi, M. H.; Soleimanifar, F.; Farid, M.; Zinatizadeh, N.; Yaslianifard, S. Investigation of enterococcus faecalis population in patients with polyp and colorectal cancer in comparison of healthy individuals. *Arq. Gastroenterol.* **2019**, *56*, 141–145.
- (6) Wang, X.; Yang, Y.; Huycke, M. M. Commensal-infected macrophages induce dedifferentiation and reprogramming of epithelial cells during colorectal carcinogenesis. *Oncotarget* **2017**, *8*, 102176–102190.
- (7) Lucas, C.; Salesse, L.; Hoang, M. H. T.; Bonnet, M.; Sauvanet, P.; Larabi, A.; Godfraind, C.; Gagnière, J.; Pezet, D.; Rosenstiel, P.; Barnich, N.; Bonnet, R.; Dalmasso, G.; Nguyen, H. T. T. Autophagy of Intestinal Epithelial Cells Inhibits Colorectal Carcinogenesis Induced by Colibactin-Producing *Escherichia coli* in ApcMin/+ Mice. *Gastroenterology* **2020**, *158*, 1373–1388.
- (8) Wang, C.-W.; Purkayastha, A.; Jones, K. T.; Thaker, S. K.; Banerjee, U. In vivo genetic dissection of tumor growth and the Warburg effect. *eLife* **2016**, *5*, No. e18126.
- (9) Zhang, W.; Zhang, S.-L.; Hu, X.; Tam, K. Y. Targeting tumor metabolism for cancer treatment: is pyruvate dehydrogenase kinases

(PDKs) a viable anticancer target? *Int. J. Biol. Sci.* **2015**, *11*, 1390–1400.

(10) Mishra, D.; Banerjee, D. Lactate dehydrogenases as metabolic links between tumor and stroma in the tumor microenvironment. *Cancers* **2019**, *11*, 750.

(11) Atas, E.; Oberhuber, M.; Kenner, L. The Implications of PDK1–4 on Tumor Energy Metabolism, Aggressiveness and Therapy Resistance. *Front. Oncol.* **2020**, *10*, 147.

(12) Feng, Y.; Xiong, Y.; Qiao, T.; Li, X.; Jia, L.; Han, Y. Lactate dehydrogenase A: A key player in carcinogenesis and potential target in cancer therapy. *Cancer Med.* **2018**, *7*, 6124–6136.

(13) Stacpoole, P. W. Therapeutic targeting of the pyruvate dehydrogenase complex/pyruvate dehydrogenase kinase (PDC/PDK) axis in cancer. *J. Natl. Cancer Inst.* **2017**, *109*, djx071.

(14) Kwak, C.-H.; Jin, L.; Han, J. H.; Han, C. W.; Kim, E.; Cho, M.; Chung, T.-W.; Bae, S.-J.; Jang, S. B.; Ha, K.-T. Ilimaquinone induces the apoptotic cell death of cancer cells by reducing pyruvate dehydrogenase kinase 1 activity. *Int. J. Mol. Sci.* **2020**, *21*, 6021.

(15) Rani, R.; Kumar, V. Recent update on human lactate dehydrogenase enzyme 5 (h LDH5) inhibitors: a promising approach for cancer chemotherapy: miniperspective. *J. Med. Chem.* **2016**, *59*, 487–496.

(16) Deng, X.; Wang, Q.; Cheng, M.; Chen, Y.; Yan, X.; Guo, R.; Sun, L.; Li, Y.; Liu, Y. Pyruvate dehydrogenase kinase 1 interferes with glucose metabolism reprogramming and mitochondrial quality control to aggravate stress damage in cancer. *J. Cancer* **2020**, *11*, 962–973.

(17) Urbańska, K.; Orzechowski, A. Unappreciated role of LDHA and LDHB to control apoptosis and autophagy in tumor cells. *Int. J. Mol. Sci.* **2019**, *20*, 2085.

(18) Zhu, X.; Xuan, Z.; Chen, J.; Li, Z.; Zheng, S.; Song, P. How DNA methylation affects the Warburg effect. *Int. J. Biol. Sci.* **2020**, *16*, 2029–2041.

(19) Luo, Y.; Ma, J.; Lu, W. The significance of mitochondrial dysfunction in cancer. *Int. J. Mol. Sci.* **2020**, *21*, 5598.

(20) Zhang, T.; Jiang, J.; Liu, J.; Xu, L.; Duan, S.; Sun, L.; Zhao, W.; Qian, F. MK2 Is Required for Neutrophil-Derived ROS Production and Inflammatory Bowel Disease. *Front. Med.* **2020**, *7*, 207.

(21) Basak, D.; Uddin, M. N.; Hancock, J. The Role of Oxidative Stress and Its Counteractive Utility in Colorectal Cancer (CRC). *Cancers* **2020**, *12*, 3336.

(22) Safarov, S.; Pulatov, E.; Kukaniev, M. A.; Kolshorn, H.; Meier, H. Ring-expansion of 5-methylene-thiazolidine-2-thione with hydrazine. *J. Heterocycl. Chem.* **2009**, *46*, 552–554.

(23) Kavaliauskas, P.; Grybaite, B.; Mickevicius, V.; Petraitiene, R.; Grigaleviciute, R.; Planciuniene, R.; Gialanella, P.; Pockevicius, A.; Petraitis, V. Synthesis ADMET properties, and in vitro antimicrobial and antibiofilm activity of 5-nitro-2-thiophenecarbaldehyde N-((E)-(5-nitrothienyl) methylidene) hydrazone (KTU-286) against *Staphylococcus aureus* with defined resistance mechanisms. *Antibiotics* **2020**, *9*, 612.

(24) Archana, S.; Pathania, S.; Chawla, P. A. Thiophene-based derivatives as anticancer agents: An overview on decade's work. *Bioorg. Chem.* **2020**, *101*, 104026.

(25) Romagnoli, R.; Prencipe, F.; Oliva, P.; Cacciari, B.; Balzarini, J.; Liekens, S.; Hamel, E.; Brancale, A.; Ferla, S.; Manfredini, S.; Zurlo, M.; Finotti, A.; Gambari, R. Synthesis and Biological Evaluation of New Antitubulin Agents Containing 2-(3',4',5'-trimethoxyanilino)-3,6-disubstituted-4,5,6,7-tetrahydrothieno[2,3-c]pyridine Scaffold. *Molecules* **2020**, *25*, 1690.

(26) Garton, A. J.; Crew, A. P. A.; Franklin, M.; Cooke, A. R.; Wynne, G. M.; Castaldo, L.; Kahler, J.; Winski, S. L.; Franks, A.; Brown, E. N.; Bittner, M. A.; Keily, J. F.; Briner, P.; Hidden, C.; Srebernak, M. C.; Pirrit, C.; O'Connor, M.; Chan, A.; Vulevic, B.; Henninger, D.; Hart, K.; Sennello, R.; Li, A.-H.; Zhang, T.; Richardson, F.; Emerson, D. L.; Castelano, A. L.; Arnold, L. D.; Gibson, N. W. OSI-930: a novel selective inhibitor of Kit and kinase insert domain receptor tyrosine kinases with antitumor activity in mouse xenograft models. *Cancer Res.* **2006**, *66*, 1015–1024.

- (27) Boutard, N.; Sabiniarz, A.; Czerwińska, K.; Jarosz, M.; Cierpich, A.; Kolasinska, E.; Wiklik, K.; Gluza, K.; Commandeur, C.; Buda, A.; Stasiowska, A.; Bobowska, A.; Galek, M.; Fabritius, C.-H.; Bugaj, M.; Palacz, E.; Mazan, A.; Zarębski, A.; Krawczyńska, K.; Żurawska, M.; Zawadzki, P.; Milik, M.; Węgrzyn, P.; Dobrzańska, M.; Brzózka, K.; Kowalczyk, P. 5-Keto-3-cyano-2,4-diaminothiophenes as selective maternal embryonic leucine zipper kinase inhibitors. *Bioorg. Med. Chem. Lett.* **2019**, *29*, 607–613.
- (28) Purkey, H. E.; Robarge, K.; Chen, J.; Chen, Z.; Corson, L. B.; Ding, C. Z.; DiPasquale, A. G.; Dragovich, P. S.; Eigenbrot, C.; Evangelista, M.; Fauber, B. P.; Gao, Z.; Ge, H.; Hitz, A.; Ho, Q.; Labadie, S. S.; Lai, K. W.; Liu, W.; Liu, Y.; Li, C.; Ma, S.; Malek, S.; O'Brien, T.; Pang, J.; Peterson, D.; Salphati, L.; Sideris, S.; Ultsch, M.; Wei, B.; Yen, I.; Yue, Q.; Zhang, H.; Zhou, A. Cell active hydroxylactam inhibitors of human lactate dehydrogenase with oral bioavailability in mice. *ACS Med. Chem. Lett.* **2016**, *7*, 896–901.
- (29) Masini, T.; Birkaya, B.; van Dijk, S.; Mondal, M.; Hekelaar, J.; Jäger, M.; Terwisscha van Scheltinga, A. C.; Patel, M. S.; Hirsch, A. K. H.; Moman, E. Furoates and thenoates inhibit pyruvate dehydrogenase kinase 2 allosterically by binding to its pyruvate regulatory site. *J. Enzyme Inhib. Med. Chem.* **2016**, *31*, 170–175.
- (30) Han, Q.; Yin, Z.; Sui, J.; Wang, Q.; Sun, Y. A Microwave-Enhanced Synthesis and Biological Evaluation of N-Aryl-5, 6, 7, 8-tetrahydrobenzo [4, 5] thieno [2, 3-d] pyrimidin-4-amines. *J. Braz. Chem. Soc.* **2019**, *30*, 1483–1497.
- (31) Mohamed, M. F.; Attia, Y. M.; Shouman, S. A.; Abdelhamid, I. A. Anticancer activities of new N-Hetaryl-2-Cyanoacetamide derivatives incorporating 4, 5, 6, 7-Tetrahydrobenzo [b] Thiophene moiety. *Anti-Cancer Agents Med. Chem.* **2017**, *17*, 1084–1092.
- (32) Elrayess, R.; Abdel Aziz, Y. M.; Elgawish, M. S.; Elewa, M.; Yassen, A. S. A.; Elhady, S. S.; Elshihawy, H. A.; Said, M. M. Discovery of Potent Dual EGFR/HER2 Inhibitors Based on Thiophene Scaffold Targeting H1299 Lung Cancer Cell Line. *Pharmaceuticals* **2021**, *14*, 9.
- (33) Sroor, F. M.; Aboelenin, M. M.; Mahrous, K. F.; Mahmoud, K.; Elwahy, A. H. M.; Abdelhamid, I. A. Novel 2-cyanoacrylamido-4,5,6,7-tetrahydrobenzo [b]thiophene derivatives as potent anticancer agents. *Arch. Pharm.* **2020**, *353*, 2000069.
- (34) Zhao, M.; Cui, Y.; Zhao, L.; Zhu, T.; Lee, R. J.; Liao, W.; Sun, F.; Li, Y.; Teng, L. Thiophene derivatives as new anticancer agents and their therapeutic delivery using folate receptor-targeting nanocarriers. *ACS Omega* **2019**, *4*, 8874–8880.
- (35) Murthy, K. N. C.; Monika, P.; Jayaprakasha, G. K.; Patil, B. S. Nanoencapsulation: An Advanced Nanotechnological Approach to Enhance the Biological Efficacy of Curcumin. *Advances in Plant Phenolics: From Chemistry to Human Health*; ACS Symposium Series; ACS: Washington, DC, 2018; pp 383–405.
- (36) Cai, G.; Wang, S.; Zhao, L.; Sun, Y.; Yang, D.; Lee, R. J.; Zhao, M.; Zhang, H.; Zhou, Y. Thiophene Derivatives as anticancer agents and their delivery to tumor cells using albumin nanoparticles. *Molecules* **2019**, *24*, 192.
- (37) Eman A. El-Helw, E. A.; Derbala, H. A.; El-Shahawi, M. M.; Salem, M. S.; Ali, M. M. Synthesis and In Vitro Antitumor Activity of Novel Chromenones Bearing Benzothiazole Moiety. *Russ. J. Bioorg. Chem.* **2019**, *45*, 42–53.
- (38) El-Sayed, N. N. E.; Almaneai, N. M.; Ben Bacha, A.; Al-Obeed, O.; Ahmad, R.; Abdulla, M.; Alafeefy, A. M. Synthesis and evaluation of anticancer, antiphospholipases, antiproteases, and antimetabolic syndrome activities of some 3H-quinazolin-4-one derivatives. *J. Enzyme Inhib. Med. Chem.* **2019**, *34*, 672–683.
- (39) Das, S.; Diyal, S.; Vinothini, G.; Perumalsamy, B.; Balakrishnan, G.; Ramasamy, T.; Dharumadurai, D.; Biswas, B. Synthesis, morphological analysis, antibacterial activity of iron oxide nanoparticles and the cytotoxic effect on lung cancer cell line. *Heliyon* **2020**, *6*, No. e04953.
- (40) Puthran, D.; Poojary, B.; Nayak, S. G.; Purushotham, N.; Bhat, M.; Hedge, H. Novel Schiff bases-based thiophenes: Design, synthesis and biological evaluation. *J. Chin. Biochem. Soc.* **2020**, *67*, 1278–1288.
- (41) Kajal, A.; Bala, S.; Kamboj, S.; Sharma, N.; Saini, V. Schiff bases: a versatile pharmacophore. *J. Catal.* **2013**, *2013*, 893512.
- (42) Tavadyan, L.; Manukyan, Z.; Harutyunyan, L.; Musayelyan, M.; Sahakyan, A.; Tonikyan, H. Antioxidant properties of selenophene, thiophene and their aminocarbonitrile derivatives. *Antioxidants* **2017**, *6*, 22.
- (43) Shah, S. T.; A Yehya, W.; Saad, O.; Simarani, K.; Chowdhury, Z.; A Alhadi, A.; Al-Ani, L. Surface functionalization of iron oxide nanoparticles with gallic acid as potential antioxidant and antimicrobial agents. *Nanomaterials* **2017**, *7*, 306.
- (44) Revanna, R. H.; Panchangam, R. K.; Bhanu, U.; Doddavenkatanna, S. Synthesis, Characterization and in vitro Antioxidant Activity of New Chiral N-boc Organotellurium Compounds, (CH₃)₃OC(O)NHCH(R)C(O)NHCH₂-CH₂Te-C₆H₄-4-OCH₃, Containing Carbamate and Peptide Groups. *J. Braz. Chem. Soc.* **2016**, *27*, 1157–1164.
- (45) Prabhu, Y. T.; Rao, K. V.; Kumari, B. S.; Kumar, V. S. S.; Pavani, T. Synthesis of Fe₃O₄ nanoparticles and its antibacterial application. *Int. Nano Lett.* **2015**, *5*, 85–92.
- (46) Taufiq, A.; Nikmah, A.; Hidayat, A.; Sunaryono, S.; Mufti, N.; Hidayat, N.; Susanto, H. Synthesis of magnetite/silica nanocomposites from natural sand to create a drug delivery vehicle. *Heliyon* **2020**, *6*, No. e03784.
- (47) Eshaghi Malekshah, R.; Fahimirad, B.; Aallaei, M.; Khaleghian, A. Synthesis and toxicity assessment of Fe₃O₄ NPs grafted by ~NH₂-Schiff base as anticancer drug: modeling and proposed molecular mechanism through docking and molecular dynamic simulation. *Drug Delivery* **2020**, *27*, 1201–1217.
- (48) Matošević, A.; Bosak, A. Carbamate group as structural motif in drugs: A review of carbamate derivatives used as therapeutic agents. *Arh. Hig. Rada Toksikol.* **2020**, *71*, 285–299.
- (49) Herbst, R. S.; Khuri, F. R. Mode of action of docetaxel—a basis for combination with novel anticancer agents. *Cancer Treat. Rev.* **2003**, *29*, 407–415.
- (50) Fujita, K.-i.; Kubota, Y.; Ishida, H.; Sasaki, Y. Irinotecan, a key chemotherapeutic drug for metastatic colorectal cancer. *World J. Gastroenterol.* **2015**, *21*, 12234–12248.
- (51) Kelly, C.; Cassidy, J. Capecitabine in the treatment of colorectal cancer. *Expert Rev. Anticancer Ther.* **2007**, *7*, 803–810.
- (52) Li, W.; Yin, Y.; Shuai, W.; Xu, F.; Yao, H.; Liu, J.; Cheng, K.; Xu, J.; Zhu, Z.; Xu, S. Discovery of novel quinazolines as potential anti-tubulin agents occupying three zones of colchicine domain. *Bioorg. Chem.* **2019**, *83*, 380–390.
- (53) Keri, R. S.; Chand, K.; Budagumpi, S.; Balappa Somappa, S.; Patil, S. A.; Nagaraja, B. M. An overview of benzo [b] thiophene-based medicinal chemistry. *Eur. J. Med. Chem.* **2017**, *138*, 1002–1033.
- (54) Mizutani, M. Y.; Takamatsu, Y.; Ichinose, T.; Nakamura, K.; Itai, A. Effective handling of induced-fit motion in flexible docking. *Proteins: Struct., Funct., Bioinf.* **2006**, *63*, 878–891.
- (55) Lipinski, C. A. Lead-and drug-like compounds: the rule-of-five revolution. *Drug Discovery Today: Technol.* **2004**, *1*, 337–341.
- (56) Gewalt, K. Heterocyclen aus CH-aciden Nitrilen, VII. 2-Amino-thiophene aus α -Oxo-mercaptanen und methylenaktiven Nitrilen. *Chem. Ber.* **1965**, *98*, 3571–3577.
- (57) Puterová, Z.; Krutošiková, A.; Végh, D. Gewalt reaction: synthesis, properties and applications of substituted 2-aminothiophenes. *ARKIVOC* **2010**, *2010*, 209.
- (58) Dong, Y.; Jiang, X.; Liu, T.; Ling, Y.; Yang, Q.; Zhang, L.; He, X. Structure-based virtual screening, compound synthesis, and bioassay for the design of Chitinase inhibitors. *J. Agric. Food Chem.* **2018**, *66*, 3351–3357.
- (59) Kim, E.-Y.; Choi, H.-J.; Park, M.-J.; Jung, Y.-S.; Lee, S.-O.; Kim, K.-J.; Choi, J.-H.; Chung, T.-W.; Ha, K.-T. Myristica fragrans suppresses tumor growth and metabolism by inhibiting lactate dehydrogenase A. *Am. J. Chin. Med.* **2016**, *44*, 1063–1079.
- (60) Bersuder, P.; Hole, M.; Smith, G. Antioxidants from a heated histidine-glucose model system. I: Investigation of the antioxidant role of histidine and isolation of antioxidants by high-performance liquid chromatography. *J. Am. Oil Chem. Soc.* **1998**, *75*, 181–187.